SAN DIEGO STATE UNIVERSITY AND

UNIVERSITY OF CALIFORNIA

Santa Barbara

Regional Streamflow Response to Wildfire in California Watersheds

A Dissertation submitted in partial satisfaction of the

requirements for the degree Doctor of Philosophy

in Geography

by

Ryan Roger Bart

Committee in charge:

Professor Allen Hope, Chair, San Diego State University

Professor Trent Biggs, San Diego State University

Professor Oliver Chadwick

Professor Christina (Naomi) Tague

June 2014

The dissertation of Ryan Roger Bart is approved.

_____

Trent Biggs

_____

Oliver Chadwick

_____

Christina (Naomi) Tague

_____

Allen Hope, Committee Chair

April 2014

Regional Streamflow Response to Wildfire in California Watersheds

by

Ryan Roger Bart

DEDICATION

For my grandfather, Bob Richards

ACKNOWLEDGEMENTS

To my wife Ana, thank you for your love and support as I worked toward finishing this dissertation. It's not easy balancing family with graduate school and you helped me through every step of the process. I hope that I can one day repay you for all the sacrifices you have made to allow me to go on this journey. I thank my son Jackson, who is my excuse to have fun every evening and every weekend. I would also like to thank my son Graham, who was kind enough to arrive shortly before I finished because he didn't want to miss the big event. Finally, thank you to my parents, Roger and Judi, who have been incredibly supportive throughout my entire academic career and continue to always be there for me.

Academically, nobody has played a larger role in mentoring me than Allen Hope. Thank you for your constant encouragement and dedication. I am also grateful for having a world-class committee to assist me; Trent Biggs, Naomi Tague and Oliver Chadwick.

I've had the privilege to work and collaborate with many great people over the years. In particular, I had a fantastic cohort: Zia Salim, Denise Goerisch, Alex Zvoleff, Sarah Wandersee, Nicole Simons, Ick Kim and Magdalena Benza (and families); whose friendships will last well beyond graduate school. To the numerous others who have helped me in both big ways and small; I am sure our paths will cross at conferences or in other places and I will be able to thank you personally.

ABBREVIATED VITA OF RYAN ROGER BART

April 2014

EDUCATION

Doctor of Philosophy in Geography, University of California, Santa Barbara & San Diego State University, June 2014 (expected)
Masters of Science in Geography, San Diego State University, August 2008
Bachelor of Science in Genetics, University of California, Davis, June 2001

PROFESSIONAL EXPERIENCE

2014: Adjunct Professor, Geography, Cuyamaca College
2014: Adjunct Professor, Geography, San Diego Mesa College
2012: Adjunct Professor, Physical Sciences Department, Southwestern College
2007-2012: Teaching Associate, Department of Geography, San Diego State University
2005-2007: Graduate Assistant, Department of Geography, San Diego State University
2001-2005: Marketing/Accounting, E-Babylon, Inc. Simi Valley, California

PUBLICATIONS

Hope A, Bart R. (2012) Synthetic monthly flow duration curves for the Cape Floristic Region, South Africa. *Water SA*, 38(2), 191-200.

Hope A, Bart R. (2012) Evaluation of a regionalization approach for daily flow duration curves in central and southern California watersheds. *Journal of the American Water Resources Association (JAWRA)*, 48(1), 123-133.

Hope A, Albers N, Bart R. (2012) Characterizing post-fire recovery of fynbos vegetation in the Western Cape Region of South Africa using MODIS data. *International Journal of Remote Sensing*, 33(4), 979-999.

Bart R, Hope A. (2010) Streamflow response to fire in large catchments of a Mediterranean-climate region using paired-catchment experiments. *Journal of Hydrology*, 388, 370-378.

AWARDS

2012 McFarland Geography Scholarship
2012 Norma Sullivan Memorial Endowed Scholarship
2011 McFarland Geography Scholarship
2007 Ned H. Greenwood Award
2006 Alvena Storm Memorial Scholarship

ABSTRACT

Regional Streamflow Response to Wildfire in California Watersheds

by

Ryan Roger Bart

As every watershed and every wildfire event is unique, streamflow response to wildfire is only representative of the specific watershed and conditions that produced the response. Most post-fire streamflow change experiments involve single watersheds, which limits extrapolation of the results beyond the particular watershed examined. A comprehensive understanding of post-fire streamflow response is needed at a regional scale to improve water resources planning and ecosystem management in California. For this dissertation, the regional effect of wildfire was examined for two different components of the streamflow hydrograph; annual streamflow yield and baseflow recession rates. Annual streamflow is a key variable for streamflow management, but high variability in post-fire annual streamflow response at the watershed scale has limited predictions of post-fire annual streamflow response at the regional scale. Baseflow recession rates are an important tool for predicting low flows, yet little is known about how baseflow recession rates

respond to wildfire at either watershed or regional scales. A mixed model was introduced to regionalize post-fire streamflow change. Mixed modeling is a statistical approach used to synthesize data containing a hierarchical structure, such as streamflow data pooled from multiple watersheds experiments. A parsimonious storage-discharge model was used to provide insight into the hydrologic processes controlling baseflow recession rates. Annual streamflow significantly increased following wildfire in California at a regional scale. This response was greatest in watersheds with higher percentages of watershed area burnt and during moderately wet years. The first-order control on baseflow recession rates in California was found to be inter-seasonal changes in antecedent storage, not wildfire. Baseflow recession rates were observed to decrease by up to an order of magnitude as antecedent storage levels increased, indicating a shift in the source of recession flows from small, quickly-recharged aquifers at the beginning of the wet season to large, seasonal aquifers as the wet season progressed. Following wildfire, baseflow recession rates significantly decreased at a regional scale, suggesting that the dominant hydrologic processes affected by fire were related to post-fire reductions in above-ground vegetation (e.g. decreased interception, decreased soil evapotranspiration, decreased groundwater evapotranspiration).

TABLE OF CONTENTS

LIST OF FIGURES

LIST OF TABLES

Chapter 1: Introduction

Wildfire is a major source of episodic land-cover change in California watersheds, dramatically transforming the landscape and initiating a complex recovery process that can take years to decades (Keeley and Keeley, 1981). Wildfire alters numerous hydrologic processes within a watershed, impacting both water resources planning and ecosystem management. The future wildfire regime in California is likely to be modified due to both anthropogenic and climate factors (Keeley and Fotheringham, 2003; Westerling and Bryant, 2008). Thus, understanding and quantifying the effects of wildfire on streamflow is increasingly critical.

Streamflow response to wildfire is dependent on the characteristics of a given watershed; the extent, severity and location of the wildfire; post-fire meteorological conditions; and the rate of post-fire recovery of vegetation and soils. Unsurprisingly, the effect of wildfire on streamflow in California has been shown to be highly variable, with some watersheds exhibiting post-fire changes in streamflow (Hoyt and Troxell, 1932; Jung et al., 2009; Loáiciga et al., 2001) and others not (Bart and Hope, 2010). Most studies of post-fire streamflow response have been examined in single watersheds. However, single-watershed studies cannot capture the range of variability in post-fire response that is needed to make robust predictions of post-fire streamflow change. There is a need for the development of regionalization approaches that can synthesize multiple watershed experiments to advance our understanding of the effects of wildfire on streamflow.

The effect of wildfire on streamflow has primarily been investigated via peak streamflow and total annual water yield (Shakesby and Doerr, 2006). Less is understood about how wildfire impacts baseflow or baseflow recession rates. Baseflow recession rates represent a measure of how baseflow, or the portion of streamflow that derives from groundwater, decreases following a recharge event. Wildfire affects baseflow recession rates primarily by decreasing post-fire transpiration from soils and groundwater through reductions in above-ground vegetation. Few post-fire change studies have addressed this component of the streamflow regime, despite baseflow recession rates being a key tool for low flow prediction (Tague and Grant, 2009) and hydrologic modeling (Tallaksen, 1995).

The objective of this dissertation is to investigate the regional effect of wildfire on streamflow, with a particular emphasis on baseflow recession rates. The dissertation is divided into three papers that each address a different aspect of this objective. Chapter 2, titled *A mixed modeling approach for regionalizing post-fire streamflow change*, examines the regional effect of wildfire on annual streamflow. A mixed modeling approach is introduced for synthesizing data from 12 paired watersheds in California. Mixed models are useful for modeling data that contains a hierarchical structure, such as annual streamflow data organized within watersheds. The goal of this paper is to regionalize post-fire annual streamflow response across California watersheds and determine how this effect may vary with the percentage of watershed area burnt, post-fire year, and annual wetness conditions.

Chapter 3, titled *Inter-seasonal variability in baseflow recession rates: The role of antecedent storage in central California watersheds*, examines the relation between antecedent storage and baseflow recession rates. A preliminary investigation into the effects of wildfire on baseflow recession rates revealed that baseflow recession rates vary inter-seasonally and that antecedent storage was the first-order control on this variability. The relation between antecedent storage and baseflow recession rates needs to be understood and accounted for prior to evaluating the effects of wildfire on baseflow recession rates. This analysis is divided into two parts, with the first part empirically examining the role of antecedent storage on baseflow recession rates in four central California watersheds. A parsimonious storage-discharge model is then employed in the second part to provide insights into the processes that produce inter-seasonal changes in baseflow recession rates.

Chapter 4, titled *The impact of wildfire on baseflow recession rates in California watersheds*, uses a mixed model to evaluate the effect of wildfire on baseflow recession rates at watershed and regional scales. The effect of antecedent storage and potential evapotranspiration (ET) on baseflow recession rate response to wildfire is also examined. This study represents the first known detailed examination of the effects of wildfire on baseflow recession rates.

The last chapter, Chapter 5, summarizes the finding of the three papers and concludes with an examination of future research questions.

1.1. References

Bart, R., Hope, A., 2010. Streamflow response to fire in large catchments of a Mediterranean-climate region using paired-catchment experiments. J. Hydrol. 388, 370–378. doi:10.1016/j.jhydrol.2010.05.016

Hoyt, W.G., Troxell, H.C., 1932. Forests and stream flow. Proc. Am. Soc. Civ. Eng. 58, 1037–1066.

Jung, H.Y., Hogue, T.S., Rademacher, L.K., Meixner, T., 2009. Impact of wildfire on source water contributions in Devil Creek, CA: evidence from end-member mixing analysis. Hydrol. Process. 23, 183–200. doi:10.1002/hyp.7132

Keeley, J.E., Fotheringham, C.J., 2003. Impact of past, present, and future fire regimes on North American Mediterranean shrublands, in: Veblen, T.T., Baker, W.L., Montenegro, G., Swetnam, T.W. (Eds.), Fire and Climatic Change in Temperate Ecosystems of the Western Americas. Springer-Verlag, New York, USA, pp. 218–262.

Keeley, J.E., Keeley, S.C., 1981. Post-fire regeneration of southern California chaparral. Am. J. Bot. 68, 524–530.

Loáiciga, H.A., Pedreros, D., Roberts, D., 2001. Wildfire-streamflow interactions in a chaparral watershed. Adv. Environ. Res. 5, 295–305.

Shakesby, R.A., Doerr, S.H., 2006. Wildfire as a hydrological and geomorphological agent. Earth Sci. Rev. 74, 269–307.

Tague, C., Grant, G.E., 2009. Groundwater dynamics mediate low-flow response to global warming in snow-dominated alpine regions. Water Resour. Res. 45, W07421. doi:200910.1029/2008WR007179

Tallaksen, L.M., 1995. A review of baseflow recession analysis. J. Hydrol. 165, 349–370. doi:10.1016/0022-1694(94)02540-R

Westerling, A.L., Bryant, B.P., 2008. Climate change and wildfire in California. Clim. Change 87, 231–249.

Chapter 2: A Mixed Modeling Approach for Regionalizing Post-Fire Streamflow Change

The effect of fire on annual streamflow has been examined in numerous watersheds studies. However, since every watershed and every fire event is unique, post-fire streamflow responses are only representative of the specific watershed and conditions that produced the response. There is a need to statistically combine the empirical results from multiple watersheds in order to estimate a regional effect of fire on streamflow. Mixed modeling is a statistical approach that is similar to regression analysis but includes random effects, which allows inferences to be drawn about a hypothetical population of watersheds from which the observed watersheds were sampled. Mixed models are useful for modeling data with a hierarchical organization (e.g. annual streamflow nested within watersheds). This study proposes a mixed-modeling approach for regionalizing the effect of fire on annual streamflow for 12 paired-watersheds in California. At a regional scale, annual streamflow in California was increased 145% (86% to 310%) during the first post-fire year in watersheds that were completely burnt. This response decreased with lower percentages of watershed area burnt and during subsequent years as vegetation recovered following fire. Annual streamflow response to fire was also sensitive to annual wetness conditions, with post-fire response being greatest during moderately wet years. The mixed

modeling approach was shown to be valuable for regionalizing the effects of land-cover change on streamflow.

2.1. Introduction

In Mediterranean-Climate Regions (MCRs) such as California, fire is an episodic form of land-cover change whose frequency and severity has increased in the past century due to the influence of humans (Keeley and Fotheringham, 2003) and may increase further with climate change (Lenihan et al., 2003; Westerling and Bryant, 2008; Williams et al., 2001). Fire removes above-ground vegetation cover and frequently produces water repellent soils ; initiating a complex recovery sequence where water repellency breaks down with successive rainfall events and burnt shrubland stands become reestablished after crowding out opportunistic herbaceous vegetation (Keeley and Keeley, 1981; Shakesby and Doerr, 2006).

Fire has been observed to impact many aspects of the streamflow regime, including peak flow, baseflow and water yield (Keller et al., 1997; Kinoshita and Hogue, 2011; McMichael and Hope, 2007). While there is a basic understanding of the individual hydrologic processes affected by fire (e.g. interception, soil infiltration, transpiration), predicting how streamflow may respond to fire for a given watershed is challenging since the effect of these processes on streamflow varies spatially from watershed to watershed and temporally as watershed conditions recover following fire. This variability stems from the uniqueness of watershed physiographic properties, meteorological conditions and vegetation types; the extent, location and

severity of the fire; and the post-fire recovery rate of vegetation and soils. Consequently, post-fire streamflow responses are largely representative of the specific watershed and conditions that produced the response.

Streamflow response to fire in MCR watersheds varies widely across watersheds, with many empirical studies observing post-fire increases in streamflow (Hoyt and Troxell, 1932; Jung et al., 2009; Lavabre et al., 1993; Loáiciga et al., 2001; Scott, 1993) and many others observing no conclusive change in streamflow (Aronica et al., 2002; Bart and Hope, 2010; Britton, 1991). Despite this inherent variability in streamflow response, the management of water resources for flood protection, water supply, water quality and the environment necessitates an understanding of post-fire effects on streamflow at a regional scale. This knowledge is essential for prediction in both gauged and ungauged watersheds.

A number of statistical models may be used to regionalize streamflow response to land-cover change such as fire; including regression, analysis of variance (ANOVA) or covariance (ANCOVA), meta-analysis and mixed modeling (Figure 1). The selection of the appropriate model depends primarily on data type and the desired inference.

The most frequently used data type is effect sizes obtained from the results of previously-conducted empirical studies in the published literature (Andréassian, 2004; Bosch and Hewlett, 1982; Brown et al., 2005; Hibbert, 1966; Sahin and Hall, 1996; Stednick, 1996). Effect sizes, such as maximum or average streamflow change, are measures of the magnitude of streamflow change and are regularly reported for

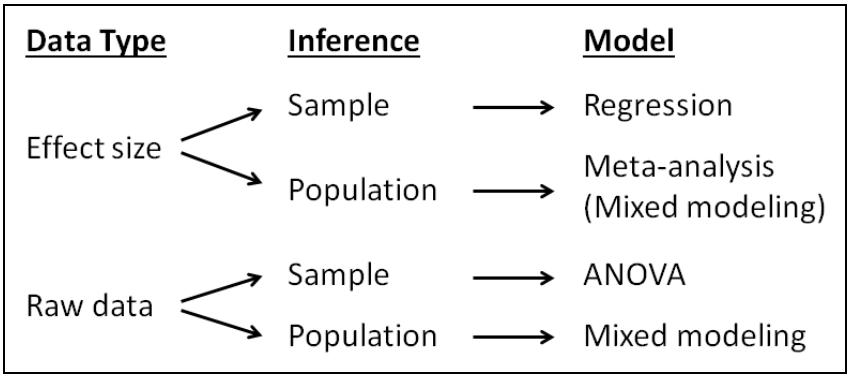

Figure 1: Flowchart for synthesizing streamflow change across multiple watersheds.

individual streamflow change studies; providing access to a broad range of locations and conditions for synthesis. A linear regression model comparing effect sizes to a predictor variable such as percentage of land-cover change has commonly been used to synthesize effect sizes. One advantage of using a linear regression model incorporating effect sizes is that the assumption of independent regression residuals is not violated when a single effect size is included from each contributing watershed study. Nonetheless, the use of a single effect size represents a loss of information relative to the original streamflow change data, which may decrease the statistical power of regionalization experiment (Hox, 2010).

An alternative data type for regionalizing streamflow change experiments that doesn't result in a loss of information is the direct combining of raw data from each individual experiment investigating changes in streamflow (Farley et al., 2005). The use of raw data theoretically leads to a more statistically powerful approach than with effect sizes since more data are available for the model. However, not all of the

additional data is informative since the generated dataset contains an embedded hierarchical structure, with streamflow data (e.g. annual streamflow) nested within watersheds. The lower level of this hierarchy (i.e. streamflow-level) is referred to as level 1 and the group- or watershed-level is referred to as level 2. Streamflow data from the same watershed are likely to be more similar than streamflow data between watersheds. Consequently, the use of a linear regression model would likely violate the assumption of residual independence. ANOVA-type models can account for watershed-level differences in streamflow data, however, implementation of these models can become problematic with large numbers of watersheds since an additional model parameter must be estimated for each additional watershed (Steele, 2008). Further, inference from ANOVA-type models assumes a balanced dataset (i.e. equal sample sizes for level-1 data) (Garson, 2012), which may not be obtainable with streamflow data.

One of the implicit goals of synthesizing multiple streamflow change studies is to infer how streamflow may respond across a study region (Figure 1). However, linear regression and ANOVA-type models treat the watersheds used in the analysis as having fixed effects, or representing all potential watersheds for which inferences are to be made. While variables with fixed effects are important for reducing model variability, for inference beyond the sample watersheds it is necessary to treat watersheds as representing a random sample of a larger population of watersheds that we would like to make inferences about. This type of variable is referred to as having random effects. Inferences based on models that include random effects in addition to

fixed effects are generally more conservative than models that include only fixed effects, lessening the likelihood of Type-1 errors, i.e., false-positive inferences of streamflow change (Borenstein et al., 2009).

Mixed modeling is a statistical approach that includes both random and fixed effects. Mixed models are useful for modeling data that is organized at multiple levels and can accommodate unbalanced datasets and large numbers of watersheds (Raudenbush and Bryk, 2002). In addition, mixed models can be used to synthesize both raw data and effect sizes from the published literature; the latter approach is referred to as meta-analysis (Hox, 2010). While mixed-modeling approaches have only recently been applied to hydrology (Chamizo et al., 2013; Clarke, 2001; Lessels and Bishop, 2013; Lopez-Moreno and Stähli, 2008; Seo et al., 2008; Webb and Kathuria, 2012; Wehrly et al., 2009), the technique is well established in the social sciences and used regularly within the ecology community (Bolker et al., 2009; Qian et al., 2010; Wagner et al., 2006).

2.2. Research objective

Despite numerous investigations into the effect of fire on annual streamflow at the watershed scale, a regional estimate of post-fire streamflow response for California has not been established. The research objective of this study was to combine streamflow data from 12 burnt watersheds and 8 proximal control (unburnt) watersheds in California in order to investigate the regional effect of fire on annual streamflow. A mixed-modeling approach was adopted based on the paired-watershed

technique, where streamflow from each burnt watershed is paired with streamflow from an unburnt watershed to act as a control.

Many of the watersheds included in this study have previously been analyzed on an individual basis for the effect of fire on streamflow (Bart and Hope, 2010; Hoyt and Troxell, 1932; Kinoshita and Hogue, 2011). Hoyt and Troxell (1932) conducted one of the first paired-watershed studies in Fish Creek following a fire in 1924 and observed a 29% increase in post-fire water yield and an increase in both peak flow and baseflow. Kinoshita and Hogue (2011) conducted a study of City Creek and Devil Canyon Creek following a large fire in 2003 and noted that both water yield and dry season baseflow increased throughout the post-fire period. Bart and Hope (2010) investigated the effect of fire on post-fire streamflow in six large (>50km^2) central California watersheds using the paired-watershed technique. Few instances of statistically significant post-fire streamflow change were reported by Bart and Hope (2010), with most post-fire streamflow falling within the uncertainty of the pre-fire calibrated model. Bart and Hope (2010) did note that the few instances of statistically significant post-fire streamflow change were associated with years of normal or above-normal annual streamflow. A similar relation between post-fire streamflow change and annual wetness conditions has also has also been observed by Feikema et al. (2013) for Australia watersheds.

Investigating the regional effect of fire on annual streamflow requires an accurate characterization of post-fire watershed conditions. For this study, four fire variables representing different post-fire watershed conditions were tested and

compared to identify the fire variable that best represents post-fire annual streamflow change. The fire variables differed in how they represented the initial change in watershed conditions following fire (i.e. burn extent) and the rate of post-fire recovery. To test the potential effect of annual wetness conditions on post-fire streamflow response, as highlighted by Bart and Hope (2010) and Feikema et al. (2013), an interaction variable was developed for the model to examine how post-fire streamflow change may vary with annual streamflow from the control watershed.

2.3. Watershed selection and data

The watersheds in this study were selected from US Geological Survey (USGS) streamflow gauges in southern and central California. Watersheds were evaluated for inclusion based on the absence of major diversions or regulations, lack of persistent winter snow cover, little urbanization or agriculture, and data record. Fire history for each watershed was obtained from the Fire and Resource Assessment Program (FRAP) (http://frap.fire.ca.gov). Paired watersheds were selected by first identifying watersheds that had been subject to a fire of at least 20% of the watershed area and also had stable land-cover conditions during the pre- and post-fire periods with no additional fires greater than 5% of the watershed area. All watersheds in the vicinity of the candidate burnt watersheds were then evaluated for also having no fires greater than 5% of the watershed area during the combined pre and post-fire period to act as a control watershed.

A total of 12 burnt watersheds were located for inclusion in the study, with 20 watersheds overall including control watersheds (Table 1). All burnt watersheds met the above selection criteria except San Antonio, Santa Paula and City which had fires during the pre-fire period of 7%, 16% and 6% of area burnt, respectively. The study watersheds are located along the Coast Range of central California and the Transverse Range of southern California (Figure 2). This region is characterized by a Mediterranean climate regime, with hot dry summer and mild wet winters. Most rainfall is generated by cyclonic frontal systems approaching from the Pacific Ocean. Since the mountains in this region are topographically very steep, precipitation totals during the wet season are driven by orographic effects.

Watershed characteristics were obtained from the Geospatial Attributes of Gages for Evaluating Streamflow (GAGES-II) database assembled by Falcone (2011) (Table 1). The area of the burnt watersheds ranged from 7 km^2 to over 600 km^2, with the smaller watersheds concentrated in the southern portion of the region. Annual precipitation totals varied from 385 mm/year to 1163 mm/year, while mean annual streamflow ranged from 22 mm/year to 753 mm/year. The lithology of the watersheds in the Transverse Range is dominated by igneous and metamorphic rocks while the watersheds in the Coast Range are primarily composed of sedimentary rocks. Soils are relatively shallow (456mm to 947mm), particularly in the steeper watersheds. Shrublands are the dominant vegetation in many of the watersheds, although grasslands, coastal sage scrub, chaparral, oak woodlands, and forests are also common (Callaway and Davis, 1993).

Table 1: Watershed characteristics

#	Watershed Name	USGS ID	Area (km^2)	Mean annual precipitation (mm)	Mean annual PET (mm)	Mean annual streamflow (mm)	Dominant geology type
1	City Creek	11055801	50.5	781	729	226	quarternary
2	Devil Canyon Creek	11063680	14.4	940	762	165	quarternary
3	Day Creek	11067000	12.0	1155	648	309	gneiss
4	Fish Creek	11084500	15.4	841	772	271	gneiss
5	Little Dalton Creek	11086500	7.2	734	804	92	gneiss
6	Arroyo Seco (South)	11098000	41.6	788	776	215	granitic
7	Santa Anita Creek	11100000	25.0	969	762	239	granitic
8	Sespe Creek	11111500	128.5	850	552	120	sedimentary
9	Santa Paula Creek	11113500	103.3	678	709	220	sedimentary
10	Coyote Creek	11117600	33.9	729	736	216	sedimentary
11	Carpinteria Creek	11119500	34.1	710	725	107	sedimentary
12	Santa Cruz Creek	11124500	191.5	831	637	96	sedimentary
13	Lopez Creek	11141280	54.0	717	741	170	sedimentary
14	Arroyo De La Cruz	11142500	106.8	906	716	460	sedimentary
15	Big Sur River	11143000	120.6	1163	640	753	granitic
16	Nacimiento River	11148900	403.5	692	745	409	sedimentary
17	San Antonio River	11149900	556.4	633	737	174	sedimentary
18	Arroyo Seco (North)	11152000	625.1	809	664	243	sedimentary
19	Los Gatos Creek	11224500	247.4	470	792	22	sedimentary
20	Cantua Creek	11253310	120.4	385	823	25	sedimentary

#	Watershed Name	Stream density (km/Km^2)	Mean slope (%)	Mean soil depth (mm)	Mean clay %	Mean silt %	Shrubland percentage
1	City Creek	1.21	34.4	650	13.2	30.6	77.5
2	Devil Canyon Creek	1.45	39.0	492	14.5	32.1	76.7
3	Day Creek	0.92	50.9	518	14.1	32.1	48.3
4	Fish Creek	1.26	39.2	493	16.5	45.7	70.8
5	Little Dalton Creek	0.77	35.9	456	18.2	49.7	87.1
6	Arroyo Seco (South)	1.13	42.8	461	17.7	48.2	70.9
7	Santa Anita Creek	1.01	44.1	475	17.3	47.6	46.6
8	Sespe Creek	1.25	26.5	573	22.1	41.3	45.9
9	Santa Paula Creek	1.18	34.4	621	23.6	44.2	55.6
10	Coyote Creek	1.10	31.2	603	25.9	44.7	46.8
11	Carpinteria Creek	1.06	32.6	643	23.8	44.7	36.3
12	Santa Cruz Creek	1.17	33.5	646	23.9	41.1	47.3
13	Lopez Creek	0.69	37.1	658	32.6	38.8	27.8
14	Arroyo De La Cruz	0.92	28.1	714	34.3	40.4	26.3
15	Big Sur River	0.98	43.6	633	14.1	31.5	33.1
16	Nacimiento River	0.99	21.3	720	22.9	36.9	40.8
17	San Antonio River	1.13	19.5	862	24.4	37.8	39.1
18	Arroyo Seco (North)	1.03	34.7	644	20.2	34.8	42.2
19	Los Gatos Creek	1.19	26.1	857	35.6	40.3	67.7
20	Cantua Creek	1.24	24.3	947	36.6	36.7	42.5

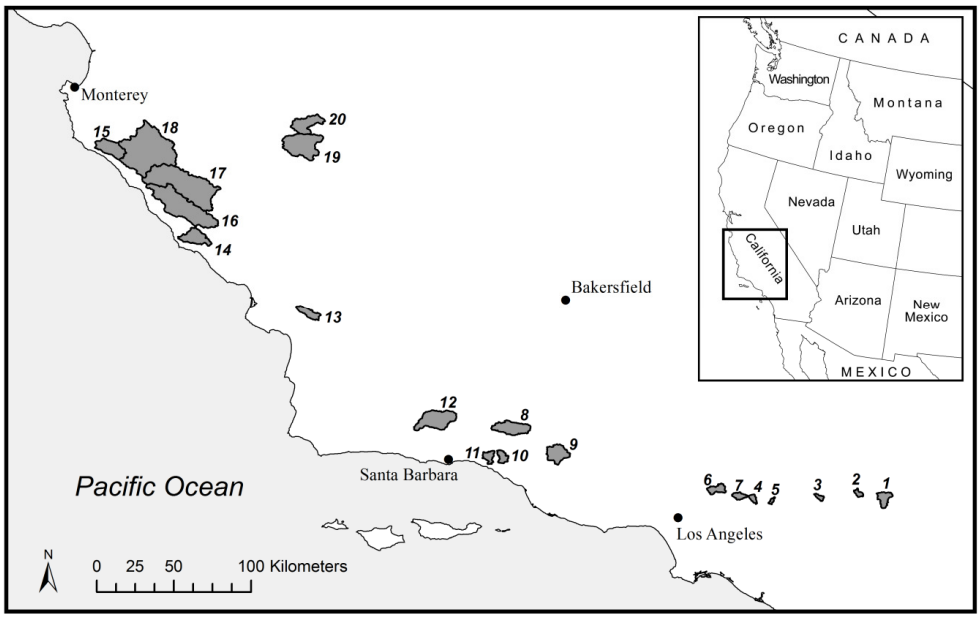

Figure 2: Location of selected research watersheds in California. Number corresponds to name and description in Table 1.

Each burnt watershed and its corresponding control watershed is listed in Table 2. The percentage of watershed area burnt ranged from 23% to 100% across all the watersheds, with higher percentages more commonly observed in smaller watersheds. Some of the control watersheds were located nearly 100 km from the burnt watershed. While differences in precipitation and watershed characteristics between the burnt and control watersheds may be expected to increase with distance between watershed pairs, Bart and Hope (2010) observed that the correlation of annual streamflow for paired watersheds at this distance in California was acceptable (R^2 >0.8). The average length of the pre-fire period was 16.6 years, ranging from 7 to 26 years. The post-fire period was monitored for up to seven years.

Table 2: Summary of paired watersheds and fire characteristics

Burnt watershed	Fire year	Area burnt (%)	Control watershed	Distance between pairs (km)	Pre-fire period	Post-fire period
Arroyo Seco (N)	1977	63	San Antonio	29	1966-1977	1978-1984
Big Sur	1977	92	Arroyo de la Cruz	72	1966-1977	1978-1979
Cantua	1979	23	Los Gatos	14	1967-1979	1980-1986
Carpinteria	1971	84	Coyote	8	1959-1971	1972-1977
City	2003	94	Arroyo Seco (S)	89	1985-2003	2004-2010
Devil Canyon	2003	97	Arroyo Seco (S)	75	1985-2003	2004-2010
Fish	1924	100	Santa Anita	9	1918-1924	1925-1931
Little Dalton	1960	100	Day	27	1940-1960	1961-1967
Lopez	1985	100	Santa Cruz	97	1968-1985	1986-1992
San Antonio	1985	31	Nacimiento	14	1972-1985	1986-1992
Santa Paula	1985	71	Santa Cruz	68	1960-1985	1986-1992
Sespe	1985	40	Santa Cruz	41	1960-1985	1986-1992

2.4. Methodology

2.4.1 Mixed modeling

For data with a hierarchical structure, dependencies are created between the lower level-1 values (hereby denoted with an *i* subscript) and the higher level-2 values (denoted with a *j* subscript) from which the level-1 values are selected. Mixed modeling, which is referred to by many different names in the literature; multilevel modeling, hierarchical modeling, generalized linear mixed modeling (GLMM), mixed-effect modeling, and meta-analysis; is a statistical approach that is similar to regression analysis but can account for hierarchies within data by partitioning model error to each level of the hierarchy using variables containing random effects. A two-level mixed model with no predictor variables (i.e. unconditional model) may be represented as

$$y_{ij} = \beta_0 + u_j + e_{ij}. \quad (1)$$

where y_{ij} is the *i*th observation of the dependent variable (i.e. annual streamflow) from the *j*th group (i.e. watershed), β_0 is the intercept of the model, u_j is the level-2 model error for the *j*th group, and e_{ij} is the level-1 model (residual) error for the *i*th observation from the *j*th group. It is generally assumed that the distribution of the model errors are normal with a mean of 0 and a variance of σ^2, such that $u_j \sim N(0, \sigma_u^2)$ and $e_{ij} \sim N(0, \sigma_e^2)$. Model error u_j represents the deviation of the level-2 groups from the overall mean, and model error e_{ij} represents the deviation of level-1 data from the corresponding level-2 group mean. This can be demonstrated by rewriting equation 1 as two equations

$$y_{ij} = \beta_{0j} + e_{ij} \quad (2a)$$

$$\beta_{0j} = \beta_0 + u_j. \quad (2b)$$

Equation 2a represents the level-1 component of the model and equation 2b represents the level-2 component.

The unconditional model in equations 1 and 2 provides a baseline estimate of the variance in the dependent variable. Predictor variables may be introduced to the

model in order to reduce this variance. A conditional mixed model with a level-1 predictor variable may be represented by

$$y_{ij} = \beta_0 + \beta_1 x_{ij} + u_j + e_{ij} \quad (3)$$

where x_{ij} is the *i*th observation of the predictor variable for the *j*th group and β_1 represents the slope of the relation between the predictor variable and the dependent variable. The fixed component is $\beta_0 + \beta_1 x_{ij}$ and the random component is $u_j + e_{ij}$. The parameters for the fixed component are β_0 and β_1 while the parameters for the random component are σ_u^2 and σ_e^2.

The model represented in equations 3 is often referred to as a random intercept model because the intercept for each level-2 group varies randomly across groups. The random intercept model assumes that the slope of the relation between a predictor variable and the dependent variable is constant across groups. This assumption may not always be appropriate. Random slope models are mixed models where the both the intercept and the slope are allowed to vary across watersheds. A random slope model for Equation 3 can be written as

$$y_{ij} = \beta_0 + \beta_1 x_{ij} + u_{0j} + u_{1j} x_{ij} + e_{ij} \quad (4)$$

or in disaggregate form as

$$y_{ij} = \beta_{0j} + \beta_{1j} x_{ij} + e_{ij} \quad (5a)$$

$$\beta_{0j} = \beta_0 + u_{0j} \tag{5b}$$

$$\beta_{1j} = \beta_1 + u_{1j}. \tag{5c}$$

The level-2 random effects are now represented by two terms, u_{0j} for the random intercept and u_{1j} for the random slope. Note that u_{1j} interacts with x_{ij}, indicating the slope of the relation between the dependent variable and the predictor variable may vary by group. A second variable is also generated from the random slope model, σ_{u01}, representing the covariance between u_{0j} and u_{1j}.

For each of the previously developed models, a single hierarchical structure was assumed to be present in the data. However, more than one hierarchical structure may exist when streamflow data is combined from multiple watersheds. Similar to how annual streamflow data from a given watershed will likely be more similar than annual streamflow from different watersheds, watersheds with annual streamflow produced from the same year will likely be more similar than annual streamflow produced from different years, as all watersheds for a given year will be subject to comparable precipitation conditions. To account for this additional hierarchy, annual streamflow is more appropriately conceptualized as having two crossed hierarchical structures instead of a single hierarchical structure, with annual streamflow being nested within both watersheds and years. This type of mixed model is referred to as

having crossed random effects (Baayen et al., 2008). An unconditional crossed random intercept model may be represented as

$$y_{i(jk)} = \beta_0 + u_{0j} + v_{0k} + e_{i(jk)} \quad (6)$$

where $y_{i(jk)}$ is the *i*th observation of the dependent variable within the cross classified *j*th watershed and *k*th year, u_{0j} and v_{0k} are the cross classified level-2 model errors, and $e_{i(jk)}$ is the level-1 residual error for the *i*th observation of the dependent variable from the cross classified *j*th watershed and *k*th year (Hox, 2010).

2.4.2 Model calibration

The standard approach for calibrating mixed models is the maximum likelihood method (Hox, 2010), which attempts to maximize a likelihood function for the optimal model fit. The maximum likelihood method is based on large-sample theory and maximum likelihood estimates and confidence intervals are considered to be very robust when level-2 sample sizes are large (Hox, 2010). However, the method has been shown to be severely biased when the level-2 sample sizes are small (Stegmueller, 2013). For small samples, it is recommended that Bayesian estimation procedures be used instead of maximum likelihood (Hox, 2010; Stegmueller, 2013). With Bayesian approaches, a prior probability distribution is developed and combined with an estimate of the likelihood of the data to produce a posterior probability

distribution, which represents the uncertainty of the model. Although the posterior distribution is generally too complicated to compute directly, Markov Chain Monte Carlo (MCMC) procedures have been developed to generate random samples from the posterior distribution. These samples, when repeated many times, can provide estimates and confidence intervals for mixed model parameters.

As the level-2 sample size for watersheds in this study was 12, a Bayesian estimation procedure was used to calibrate the model. Mixed modeling was conducted in the R programming language (www.r-project.org) using the MCMCglmm (Hadfield, 2010) and MuMIn (Bartoń, 2013) packages. An improper, non-informative prior was used to minimize the effect of the prior on the model results, although the model was observed to be relatively insensitive to the prior distribution. A Gibbs sampling algorithm was used for the MCMC walk (Hadfield, 2010) and 1,000,000 iterations with a thinning of 20 were used to calibrate each model.

The test statistic used for model selection was the Deviance Information Criterion (DIC) (Hadfield, 2010). The DIC is a generalization of the Akaike information criterion and is defined as

$$DIC = \overline{D} + p_D \tag{7}$$

where $\overline{D}$ is a measure of model fit and p_D is a measure of model complexity. $\overline{D}$ is the average deviance *D* over all MCMC iterations, with deviance is defined as

$$D = -2\ln(p(y|\theta)). \tag{8}$$

$p(y|\theta)$ is the likelihood function and θ is a parameter of the model. p_D is a measure of the effective number of parameters (Spiegelhalter et al., 2002). Models with smaller values of DIC indicate better model fit.

2.4.3 Model development and model variables

Model development for predicting annual streamflow (mm) from the burnt watershed began with a parsimonious base model and proceeded by incrementally adding more complexity to the model (Figure 3). The base model included crossed random intercepts for watershed and wateryear (October 1 to September 30), but no predictor variables (Model 1). Following the addition of each model variable, the value of the DIC statistic was evaluated to determine if the new variable improved model fit.

Annual streamflow from the control watersheds was expected to be the strongest predictor of annual streamflow from the burnt watersheds by controlling for inter-annual differences in precipitation and hydrologic behavior (Model 2). Since the relation between annual streamflow from the burnt and control watersheds was heteroscedastic and non-normal, streamflow data from both watersheds was log (base *e*) transformed for Model 2 and all subsequent models. In some cases, the log transformation of very small annual streamflow totals (less than 1 mm) produced influential points due to the amplification of very small differences in annual streamflow. Influential points were removed following the approach outlined in Bart

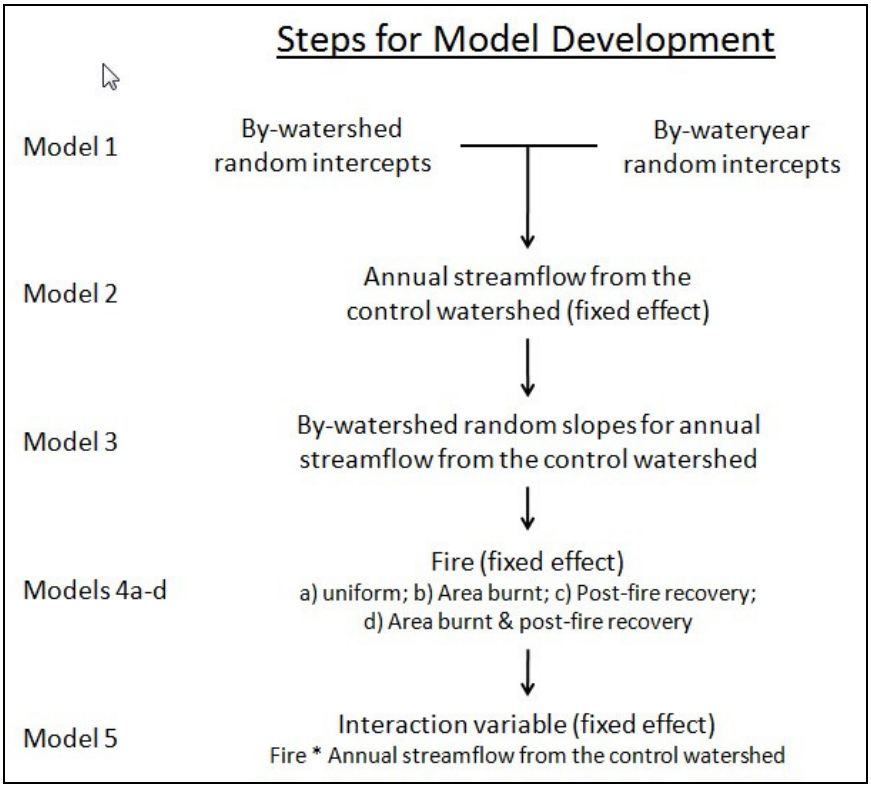

Figure 3: Steps for model development

and Hope (2010). Annual streamflow from the control watersheds was group-mean centered by subtracting the mean of the level-2 group to which each value was associated (Enders and Tofighi, 2007).

Model 3 tested whether the addition of by-watershed random slopes for annual streamflow from the control watershed provide a better model fit than the random intercepts of Model 2 (Figure 3).

Model 4 incorporated a fire variable for characterizing post-fire watershed conditions. As the post-fire recovery of watershed conditions is highly variable, there is no established approach for defining post-fire watershed conditions in California.

Some studies have treated the post-fire period as having uniform conditions for a fixed period of time (Bart and Hope, 2010; Loáiciga et al., 2001). However, an alternative approach is to have the fire variable approximate the post-fire recovery of watershed conditions. This latter approach provides a more realistic representation of post-fire watershed conditions. Further, since the effect of fire lessens with time, the subjective designation of post-fire length becomes less critical than under uniform conditions.

For this study, four fire variables representing different metrics of post-fire change and post-fire watershed recovery were tested and compared to determine which variable most accurately characterized post-fire watershed conditions. For each of the fire variables, watershed conditions during the pre-fire period were assumed to be uniform. For the post-fire period, the first variable assumed that the initial post-fire change was equal for all watersheds and that post-fire conditions were uniform throughout a 7-year period following fire (Model 4a). The second fire variable accounted for watershed to watershed differences in the initial post-fire change by weighting the post-fire period by the percentage of watershed area burnt (Model 4b). While the percentage of area burnt does not account for the severity of the fire or spatial differences from burning in hydrologically connected verses unconnected areas, it does provides a rough estimate of the differences in initial post-fire watershed conditions between watersheds. The third variable assumed that the initial post-fire change was equal for all watersheds but accounted for the temporal recovery of watershed conditions following fire by weighting the post-fire period by

the reverse scaling (i.e. 1 minus value) of a normalized post-fire vegetation recovery curve (see next paragraph) (Model 4c). The post-fire period of the fourth fire variable was weighted by both the percentage of watershed area burnt and the normalized post-fire vegetation recovery curve (Model 4d).

The normalized post-fire vegetation recovery curve was derived from two remote sensing studies in central California (Hope et al., 2007; McMichael et al., 2004) (Figure 4). This curve was used for characterizing the post-fire recovery for each individual watershed since the fires in this study date as far back as the 1920s and remotely-sensed measures of vegetation recovery cannot be used ubiquitously across all fire events. McMichael et al. (2004) used a chronosequence technique to develop a post-fire recovery curve for leaf-area index (LAI) while Hope et al. (2007) used a NDVI time-series to directly produce a recovery curve for vegetation stands. These studies observed that post-fire recovery of above-ground vegetation ranged from 10 to 15 years following fire. The normalized post-fire vegetation recovery curve did not incorporate the post-fire recovery of soils since no large scale estimate of soil recovery was available. As soils may be expected to recover faster than vegetation (Shakesby and Doerr, 2006), this omission may cause the model to underestimate post-fire streamflow response during years when streamflow is affected by post-fire changes in soil hydrophobicity and overestimate post-fire streamflow response when streamflow is unaffected.

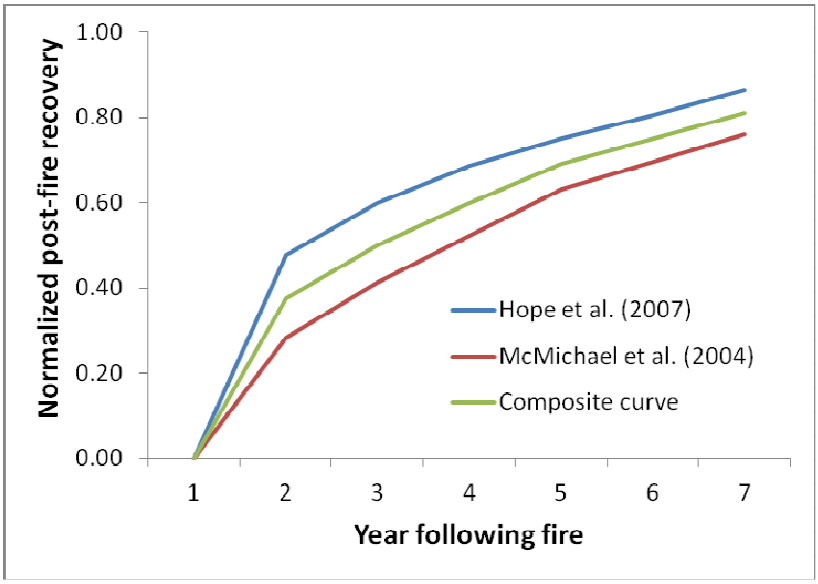

Figure 4: Normalized post-fire vegetation recovery curve. (Figure adapted from Figure 2 in McMichael et al. (2004) and Figure 4 in Hope et al. (2007)).

The final model (Model 5) investigated how the effect of fire varies from wateryear to wateryear with changes in annual wetness conditions via an interaction variable (Figure 3). The interaction variable was generated from the product of the two interacting variables; the fire variable introduced in Model 4 and annual streamflow from the control watershed.

2.5. Results

Plots of pre- and post-fire annual streamflow totals for each of the twelve burnt and control watersheds are displayed in Figure 5. A linear least-square regression model (solid line) fitted to the pre-fire data is plotted for each watershed pair. Linear regression represents the standard approach for modeling individual

paired-watershed relations. For some of the burnt watersheds, the deviations of the post-fire annual streamflow data about the regression line did not exceed the variability of the pre-fire data, indicating that post-fire change may not be detectable for some paired watersheds on an individual basis (Bart and Hope, 2010). However, across all 12 watershed pairs, 74.7% of post-fire annual streamflow points plotted above the pre-fire linear regression line, implying that on a regional scale, post-fire annual streamflow may have increased in the burnt watersheds relative to the control watersheds.

Both the intercept and slope of the linear regression models in Figure 5 differed for each watershed pair. Thus at the regional scale, a linear regression model based on all data points from all watersheds would likely be inappropriate for modeling post-fire streamflow response since streamflow from each watershed pair would be correlated. The plots also suggested that a random slope model, as opposed to a random intercept model, may be necessary to accurately characterize the combined streamflow data.

Model development was initiated with a parsimonious base model consisting of crossed random intercepts for watershed and wateryear with no predictor variables. This model was found to be unstable, with the level-2 variance for wateryear not converging on a single solution. This non-convergence may possibly be related to the percentage of total model variance explained by wateryear being very small (less than 5%). Since incorporating wateryear as a random intercept did not improve model fit

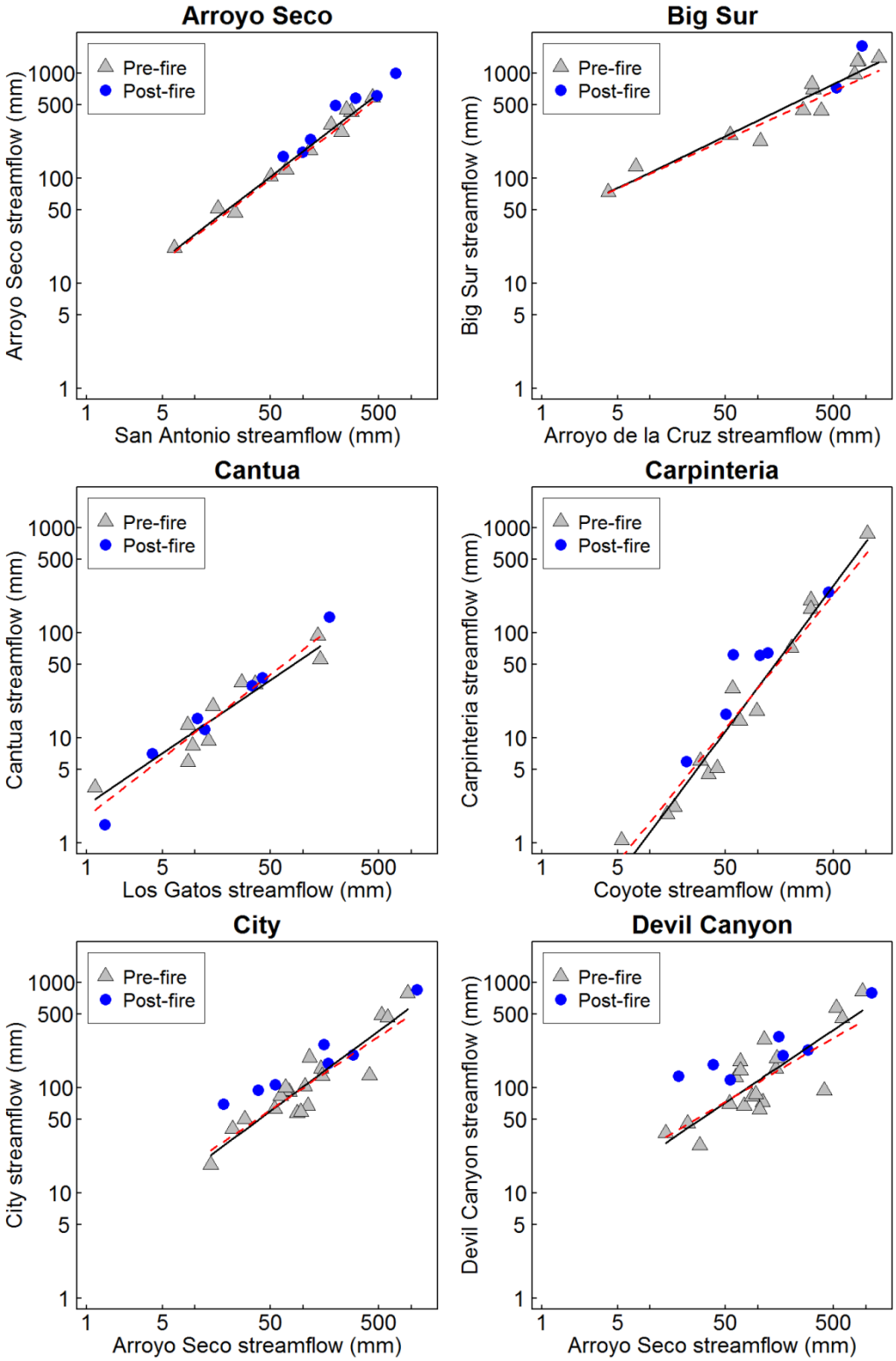
Arroyo Seco
Pre-fire
Post-fire
Arroyo Seco streamflow (mm)
San Antonio streamflow (mm)
Big Sur
Big Sur streamflow (mm)
Arroyo de la Cruz streamflow (mm)
Cantua
Cantua streamflow (mm)
Los Gatos streamflow (mm)
Carpinteria
Carpinteria streamflow (mm)
Coyote streamflow (mm)
City
City streamflow (mm)
Arroyo Seco streamflow (mm)
Devil Canyon
Devil Canyon streamflow (mm)
Arroyo Seco streamflow (mm)
1
5
10
50
100
500
1000

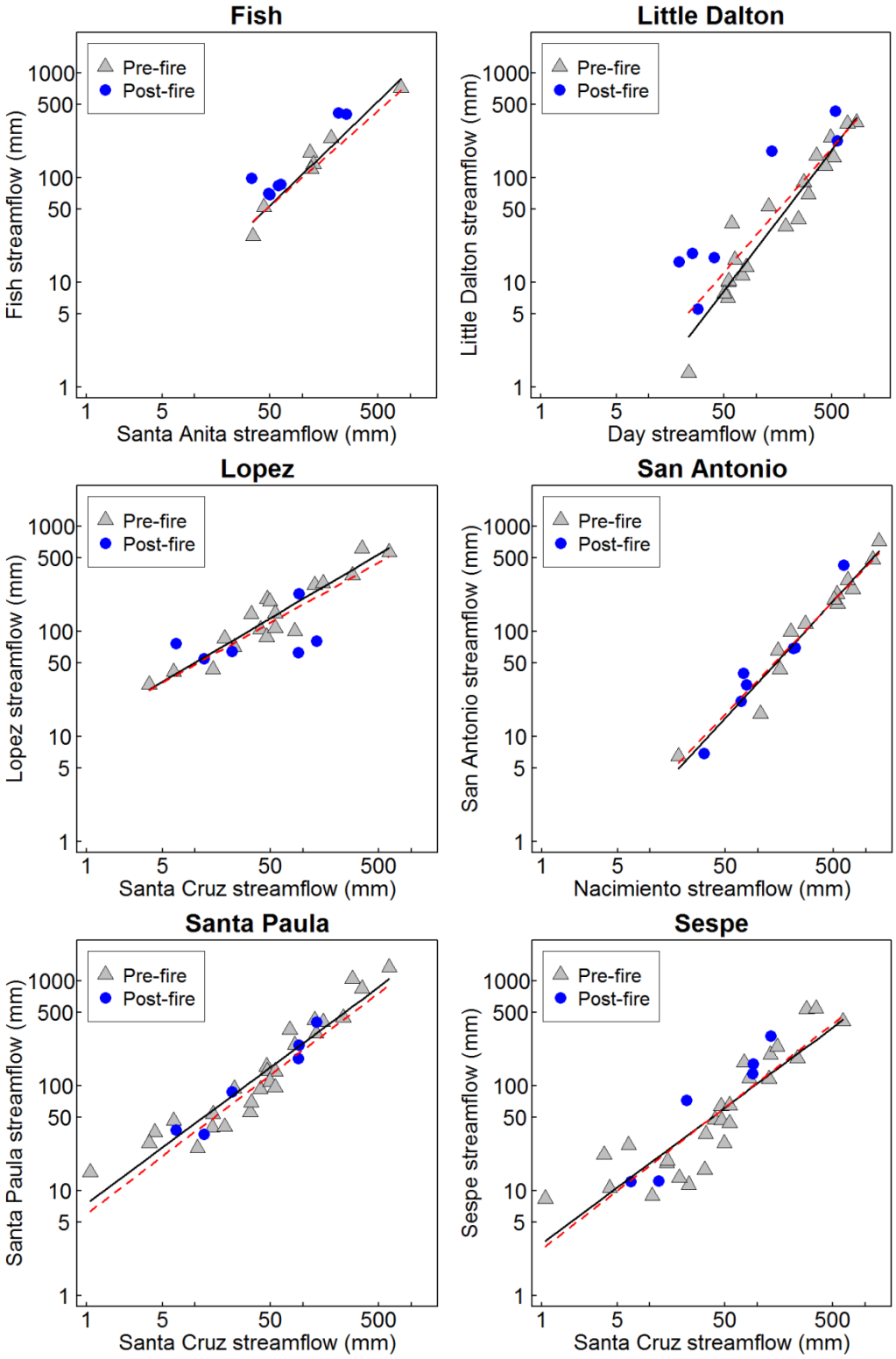
Fish
Pre-fire
Post-fire
Fish streamflow (mm)
Santa Anita streamflow (mm)
Little Dalton
Little Dalton streamflow (mm)
Day streamflow (mm)
Lopez
Lopez streamflow (mm)
Santa Cruz streamflow (mm)
San Antonio
San Antonio streamflow (mm)
Nacimiento streamflow (mm)
Santa Paula
Santa Paula streamflow (mm)
Santa Cruz streamflow (mm)
Sespe
Sespe streamflow (mm)
Santa Cruz streamflow (mm)
1
5
10
50
100
500
1000

Figure 5: Plots of annual streamflow from the burnt watershed (y-axis) against annual streamflow from the control watershed (x-axis). Solid black line represents linear regression model fitted to pre-fire annual streamflow. Dashed red line represents predicted pre-fire relation between the control and burnt watersheds using Model 4d.

but instead increased model instability, this variable was removed from the base model and all subsequent models.

The values representing the mode and 95% credible (i.e. confidence) intervals for each fixed and random parameter in Models 1-3, as well as the model DIC, are displayed in Table 3. The new base model consisting of a random intercept model grouped by watershed with no predictor variables is shown as Model 1. For this model, the only fixed effect calculated was the intercept, which represents the population mean for logged annual streamflow from the burnt watersheds, adjusted for the hierarchical structure of the data. Two random effects were produced by the base model, a level-1 residual variance σ_e^2 and a level-2 intercept variance σ_u^2. Inter-watershed differences in the intercept of the mixed model accounted for 31.6% of the variance in annual streamflow from the burnt watersheds, while the remainder of the variance was attributable to intra-watersheds processes. The DIC for Model 1 was 873.7.

The addition of annual streamflow from the control watersheds as a predictor variable to the mixed model is displayed as Model 2 (Table 3). The predictor variable improved model fit, with the DIC decreasing to 455.5. The inclusion of annual streamflow from the control watersheds altered the partitioning of variance within the

Table 3: Estimate (mode) with 95% credible intervals of parameters for Models 1-3.

Characteristic	Model 1	Model 2	Model 3
Fixed effects			
Intercept	4.539 (3.868 to 5.067)	4.313 (3.729 to 5.012)	4.349 (3.660 to 5.019)
Control Q (log, centered at 4.331)		0.814 (0.760 to 0.861)	0.835 (0.666 to 1.014)
Random effects			
Level-2 variance (Intercept)	0.663 (0.277 to 2.118)	0.897 (0.367 to 2.390)	0.970 (0.378 to 2.850)
Level-2 variance (Slope)			0.053 (0.020 to 0.182)
Level-2 covariance (Intercept & slope)			-0.139 (-0.555 to 0.006)
Level-1 variance (Residual)	1.437 (1.204 to 1.704)	0.288 (0.254 to 0.358)	0.216 (0.177 to 0.254)
Total variance	2.100	1.185	1.186
Level-2 variance/ Total variance	31.6%	75.7%	81.8%
DIC	873.7	455.5	372.0

model, with over 75% of the model variance now accounted for by inter-watershed differences in the intercept. The residual variance of the model was reduced to approximately one-fifth the Model 1 variance.

In Model 3, the slope of the relation between annual streamflow from the control watersheds and annual streamflow from the burnt watersheds was allowed to vary in addition to the intercept (Table 3). This inclusion of the random slope improved the fit of Model 3, with DIC decreasing to 372.0. Variance associated with random effects has a slightly different interpretation under a random slope model than a random intercept model, as variance is now dependent on the value of annual streamflow from the control watershed (Equation 4). The values displayed in Model 3 represent the variance at the group mean centered value of annual streamflow from the control watershed (76 mm). At this value, total variance for Model 3 remained approximately the same as Model 2, although residual variance decreased.

The model results from the addition of four different fire predictor variables; uniform conditions (Model 4a), area burnt (Model 4b), post-fire recovery (Model 4c), and both area burnt and post-fire recovery (Model 4d); are shown in Table 4. Model 4a showed a decrease in DIC to 348.1 and had a fire coefficient value of 0.305. The antilog of this coefficient value equates to a 36% (20% to 53%) increase in annual streamflow for each post-fire year. Model 4b showed a slightly improved model fit (DIC = 344.1) and an increase in post-fire annual streamflow of 52% (30% to 76%) assuming 100% burnt. For watersheds that burn less than 100%, the corresponding post-fire streamflow response would be smaller. Model 4c further improved model fit

Table 4: Estimate (mode) with 95% credible intervals of parameters for Models 4-5.

Characteristic	Model 4a	Model 4b	Model 4c	Model 4d	Model 5
Fixed effects					
Intercept	4.368 (3.613 to 4.982)	4.356 (3.606 to 4.934)	4.327 (3.599 to 4.966)	4.325 (3.636 to 4.968)	4.322 (3.630 to 4.993)
Control Q (log, centered at 4.331)	0.840 (0.660 to 1.018)	0.821 (0.662 to 1.022)	0.826 (0.661 to 1.021)	0.843 (0.658 to 1.017)	0.864 (0.689 to 1.049)
Fire (Uniform)	0.305 (0.182 to 0.427)				
Fire (Area burnt)		0.419 (0.264 to 0.566)			
Fire (Post-fire recovery)			0.621 (0.432 to 0.840)		
Fire (Area burnt & post-fire recovery)				0.859 (0.608 to 1.126)	0.896 (0.623 to 1.130)
Fire * Control Q (log, centered at 4.331)					-0.258 (-0.476 to -0.074)
Random effects					
Level-2 variance (Intercept)	0.960 (0.405 to 2.936)	0.939 (0.399 to 2.847)	0.891 (0.392 to 2.900)	0.865 (0.379 to 2.807)	0.887 (0.393 to 2.866)
Level-2 variance (Slope)	0.065 (0.024 to 0.194)	0.057 (0.023 to 0.194)	0.057 (0.023 to 0.194)	0.059 (0.022 to 0.195)	0.064 (0.022 to 0.202)
Level-2 covariance (Intercept & slope)	-0.167 (-0.570 to 0.009)	-0.136 (-0.569 to 0.004)	-0.150 (-0.584 to 0.001)	-0.150 (-0.579 to 0.003)	-0.141 (-0.563 to 0.011)
Level-1 variance (Residual)	0.196 (0.161 to 0.231)	0.190 (0.159 to 0.227)	0.182 (0.154 to 0.221)	0.180 (0.151 to 0.216)	0.174 (0.146 to 0.209)
Total variance	1.156	1.129	1.073	1.045	1.045
Level-2 variance/ Total variance	83.0%	83.2%	83.0%	82.8%	82.8%
DIC	348.1	344.1	335.2	328.6	322.3

with a reduction in DIC to 335.2. The improved fit of Model 4c relative to Model 4b suggests that accounting for the post-fire recovery of watershed conditions is more important than accounting for watershed differences in the percentage of area burnt. Post-fire annual streamflow in Model 4c increased 86% (54% to 132%) during the first post-fire wateryear. Model 4d, which accounted for both area burnt and the post-fire recovery of watershed conditions, provided the best model fit (DIC = 328.6). This model predicted that the regional effect of fire during the first post-fire wateryear for a watershed that is 100% burnt would be a 136% (84% to 308%) increase in annual streamflow.

For a given percentage of area burnt and for a given post-fire year, the effect of fire on annual streamflow was assumed to be equal under all conditions using Model 4d. An interaction variable between the fire variable from Model 4d and antecedent streamflow from the control watershed was included in Model 5 to test whether the effect of fire on annual streamflow varies with annual wetness conditions (Table 4). Model 5 provided the best fit in the study, with DIC decreasing to 322.3. The fire variable in Model 5 predicted that post-fire annual streamflow would increase 145% (86% to 310%) during the first post-fire year assuming 100% area burnt. This value represented the effect of fire on annual streamflow under average annual wetness conditions for the region, specifically when annual streamflow from the control watershed was at its centered mean value of 76 mm. The interaction variable modified this effect when annual streamflow values for the control watershed were above or below the centered value. On a percent change basis, the effect of fire

on annual streamflow decreased by 16% (5% to 28%) for every doubling of annual streamflow from the control watershed (Figure 6a). However, when the percentage change in annual streamflow was transformed into a volumetric (mm) change, only small increases in post-fire annual streamflow were observed during dry years. Post-fire annual streamflow response increased with annual wetness conditions until reaching a maximum of 197 mm when annual streamflow from the control watershed was 620 mm (Figure 6b). Following this maximum, post-fire streamflow response began to decrease again. The predicted streamflow response to fires with less than 100% of the watershed area burnt follows a similar pattern, but response was scaled proportionally downward.

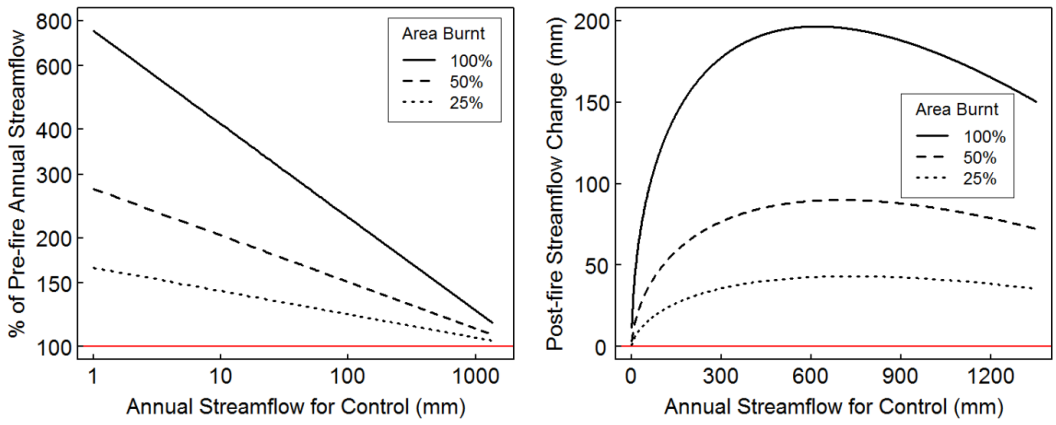

Figure 6: Predicted change (% and mm) in annual flow during the first post-fire year, adjusted for annual wetness conditions.

2.6. Discussion

All four of the fire variables tested in Models 4a-d had 95% credible intervals that were positive (Table 4). These results provide strong evidence that, despite the variability observed in post-fire response at a watershed scale, post-fire annual streamflow increases relative to pre-fire annual streamflow at a regional scale. Nonetheless, there is still large uncertainty in quantifying the regional increase in post-fire annual streamflow (e.g. 84% to 308% for Model 4d), reflecting the limitation of using only 12 watershed pairs to estimate a regional-level response. The post-fire responses in this study represent a best estimate given the available data. The coefficient values increased from Model 4a to Model 4d in line with expectations. The fire variable in Model 4a showed the smallest post-fire increase (36%) since post-fire response was distributed equally over all watersheds and the entire 7-year post-fire period. The fire variable in Model 4d, on the other hand, showed a much sharper post-fire increase in annual streamflow (136%) since this increase was only applicable to the first post-fire year in watersheds that were 100% burnt.

Annual streamflow response to fire was lowest during dry years, greatest during moderately wet years, and then slowly decreased for very wet years (Figure 6b). A possible physical explanation for these results relates to the interaction between soil drainage and rooting depth (Wilcox et al., 2006). During dry years, the storage capacity within the shallow rooting zone of the herbaceous vegetation that dominate early post-fire succession may be sufficient to transpire all available soil

water, minimizing the transpirational differences between post-fire herbaceous vegetation and pre-fire chaparral and trees. During years with moderate levels of wetness, the effect of differences in pre- and post-fire rooting depth on vegetation transpiration becomes more pronounced as water that may be available for transpiration under pre-fire conditions moves beyond the rooting zone under post-fire conditions. These differences in transpiration increase the likelihood that post-fire annual streamflow will increase at moderate wetness levels. A similar effect has been noted by Zhang et al. (2001), who observed that the effect of vegetation rooting depth on mean annual transpiration was greatest for intermediate wetness conditions. This result also supports observations made by Bart and Hope (2010) and Feikema et al. (2013) for the role of annual wetness on post-fire streamflow response. For very wet years, transpiration becomes slightly less sensitive to differences in pre- and post-fire rooting depths as precipitation frequency becomes sufficient to sustain transpiration at potential levels for both pre- and post-fire vegetation. Nevertheless, soil moisture held beyond the rooting depth of herbaceous vegetation but within the rooting zone of pre-fire vegetation at the end of the California wet season may still produce differences in transpiration.

The mixed modeling approach used in this study appears to be a viable technique for modeling post-fire changes in annual streamflow at a regional scale. The random slope models provided good fit to the paired watershed data. For example, the predicted pre-fire relation between annual streamflow from the burnt watershed and annual streamflow from the control watershed using Model 4d was

similar to the linear regression models developed from each individual watershed pair (Figure 5 - red dashed line). This demonstrates that the mixed model was able to account for watershed to watershed differences in the intercept and slope of the paired-watershed relation.

Still, the findings of this study should be evaluated in the context of the assumptions and uncertainty of the modeling approach. First, a single hierarchical structure grouped by watershed was used instead of the crossed random effects structure containing both watersheds and wateryear, since the latter model structure was observed to be unstable. While this difference would not be expected to appreciably alter the results of this study since the variance explained by wateryear was minimal, accounting for this variable may be important in other studies. Second, the mixed modeling approach assumed that the watersheds used in calibration were a random sample taken from a larger population of watersheds. The watersheds in this study were instead selected based on available USGS gauged watersheds meeting pre-established criteria with the assumption that the selected watersheds were representative of other watersheds in the region. The effect of this bias in sampling scheme on model inference is unclear. Third, no attempts were made in this study to account for spatial correlation between watersheds, in part due to the difficulty in accurately characterizing spatial correlation with only 12 burnt watersheds. In future studies, particularly with larger sample sizes, spatial correlation between watersheds may need to be addressed (Banerjee et al., 2003). Finally, no validation procedure was conducted in this study due to the limited sample size. While the DIC statistic

provides an estimate of the calibrated model fit, it has been found to overfit models in some cases (Plummer, 2008). A more robust validation procedure (e.g. cross validation) may provide a better estimate of model fit (Hope and Bart, 2012).

2.7. Conclusions

The mixed modeling approach used in this study was developed to account for the hierarchical structure of streamflow data when data from multiple watersheds are pooled together. This approach permitted the regional analysis of post-fire annual streamflow change in California watersheds. The best mixed model for predicting post-fire streamflow change was a random slope model with a fire variable that accounted for both differences in watershed area burnt and post-fire vegetation recovery, as well as an interaction variable describing the influence of annual wetness conditions. At a regional scale, post-fire annual streamflow was predicted to increase 145% (86% to 310%) during the first post-fire year assuming 100% burnt and average annual wetness conditions. This response varied from year to year based on annual wetness conditions, with the effect of fire being smallest during dry years, greatest during moderately wet years, and slowly decreasing during very wet years.

The mixed modeling approach is particularly well suited for exploiting large watershed datasets (e.g. MOPEX); however this study has demonstrated that mixed models may also be used when the number of the watersheds available for synthesis is limited. While the 12 watersheds used for this study is arguably inadequate for establishing a robust estimate of the true regional effect of wildfire on annual

streamflow, it is substantially more informative than results based on single watershed experiments, as is most commonly used for investigating post-fire streamflow response. Further, future research may wish to extend this modeling approach to the effect of other types of land-cover/ climate change on streamflow.

2.8. References

Andréassian, V., 2004. Waters and forests: from historical controversy to scientific debate. Journal of Hydrology 291, 1–27.

Aronica, G., Candela, A., Santoro, M., 2002. Changes in the hydrological response of two Sicilian basins affected by fire, in: van Lanen, H.A.J., Demuth, S. (Eds.), FRIEND 2002- Regional Hydrology: Bridging the Gap Between Research and Practice, IAHS Publ. 274. IAHS Press, Wallingford, UK, pp. 163–169.

Baayen, R.H., Davidson, D.J., Bates, D.M., 2008. Mixed-effects modeling with crossed random effects for subjects and items. Journal of memory and language 59, 390–412.

Banerjee, S., Gelfand, A.E., Carlin, B.P., 2003. Hierarchical modeling and analysis for spatial data. CRC Press.

Bart, R., Hope, A., 2010. Streamflow response to fire in large catchments of a Mediterranean-climate region using paired-catchment experiments. Journal of Hydrology 388, 370–378.

Bartoń, K., 2013. MuMIn: multi-model inference.

Bolker, B.M., Brooks, M.E., Clark, C.J., Geange, S.W., Poulsen, J.R., Stevens, M.H.H., White, J.-S.S., 2009. Generalized linear mixed models: a practical guide for ecology and evolution. Trends in ecology & evolution 24, 127–135.

Borenstein, M., Hedges, L.V., Higgins, J.P.T., Rothstein, H.R., 2009. Introduction to meta-analysis. John Wiley & Sons.

Bosch, J.M., Hewlett, J.D., 1982. A review of catchment experiments to determine the effect of vegetation changes on water yield and evapotranspiration. Journal of Hydrology 55, 3–23.

Britton, D.L., 1991. Fire and the chemistry of a South African mountain stream. Hydrobiologia 218, 177–192.

Brown, A.E., Zhang, L., McMahon, T.A., Western, A.W., Vertessy, R.A., 2005. A review of paired catchment studies for determining changes in water yield resulting from alterations in vegetation. Journal of Hydrology 310, 28–61.

Callaway, R.M., Davis, F.W., 1993. Vegetation Dynamics, Fire, and the Physical Environment in Coastal Central California. Ecology 74, 1567–1578.

Chamizo, S., Cantón, Y., Lázaro, R., Domingo, F., 2013. The role of biological soil crusts in soil moisture dynamics in two semiarid ecosystems with contrasting soil textures. Journal of Hydrology 489, 74–84.

Clarke, R.T., 2001. Separation of year and site effects by generalized linear models in regionalization of annual floods. Water resources research 37, 979–986.

Enders, C.K., Tofighi, D., 2007. Centering predictor variables in cross-sectional multilevel models: a new look at an old issue. Psychological methods 12, 121.

Falcone, J.A., 2011. GAGES-II: geospatial attributes of gages for evaluating streamflow. Digital spatial data set.

Farley, K.A., Jobbágy, E.G., Jackson, R.B., 2005. Effects of afforestation on water yield: a global synthesis with implications for policy. Global Change Biology 11, 1565–1576.

Feikema, P.M., Sherwin, C.B., Lane, P.N.J., 2013. Influence of climate, fire severity and forest mortality on predictions of long term streamflow: Potential effect of the 2009 wildfire on Melbourne's water supply catchments. Journal of Hydrology 488, 1–16.

Garson, G.D., 2012. Hierarchical linear modeling: Guide and applications. Sage.

Hadfield, J.D., 2010. MCMC methods for multi-response generalized linear mixed models: the MCMCglmm R package. Journal of Statistical Software 33, 1–22.

Hibbert, A.R., 1966. Forest treatment effects on water yield, in: Proceedings of a National Science Foundation Advanced Science Seminar, International Symposium on Forest Hydrology. Pergamon Press, USA. pp. 527–543.

Hope, A., Bart, R., 2012. Synthetic monthly flow duration curves for the Cape Floristic Region, South Africa. Water SA 38, 191–200.

Hope, A., Tague, C., Clark, R., 2007. Characterizing post-fire vegetation recovery of California chaparral using TM/ETM+ time-series data. Int. J. of Remote Sensing 28, 1339–1354.

Hox, J., 2010. Multilevel analysis: Techniques and applications. Routledge Academic.

Hoyt, W.G., Troxell, H.C., 1932. Forests and stream flow. Proceedings of the American Society of Civil Engineers 58, 1037–1066.

Jung, H.Y., Hogue, T.S., Rademacher, L.K., Meixner, T., 2009. Impact of wildfire on source water contributions in Devil Creek, CA: evidence from end-member mixing analysis. Hydrol. Process. 23, 183–200.

Keeley, J.E., Fotheringham, C.J., 2003. Impact of past, present, and future fire regimes on North American Mediterranean shrublands, in: Veblen, T.T., Baker, W.L., Montenegro, G., Swetnam, T.W. (Eds.), Fire and Climatic Change in Temperate Ecosystems of the Western Americas. Springer-Verlag, New York, USA, pp. 218–262.

Keeley, J.E., Keeley, S.C., 1981. Post-fire regeneration of southern California chaparral. American Journal of Botany 68, 524–530.

Keller, E.A., Valentine, D.W., Gibbs, D.R., 1997. Hydrological response of small watersheds following the Southern California Painted Cave Fire of June 1990. Hydrological Processes 11, 401–414.

Kinoshita, A.M., Hogue, T.S., 2011. Spatial and temporal controls on post-fire hydrologic recovery in Southern California watersheds. Catena 87, 240–252.

Lavabre, J., Torres, S., Cernesson, F., 1993. Changes in the hydrological response of a small Mediterranean basin a year after a wildfire. Journal of Hydrology 142, 273–299.

Lenihan, J.M., Drapek, R., Bachelet, D., Neilson, R.P., 2003. Climate change effects on vegetation distribution, carbon, and fire in California. Ecological Applications 13, 1667–1681.

Lessels, J.S., Bishop, T.F.A., 2013. Estimating water quality using linear mixed models with stream discharge and turbidity. Journal of Hydrology 498, 13–22.

Loáiciga, H.A., Pedreros, D., Roberts, D., 2001. Wildfire-streamflow interactions in a chaparral watershed. Advances in Environmental Research 5, 295–305.

Lopez-Moreno, J.I., Stähli, M., 2008. Statistical analysis of the snow cover variability in a subalpine watershed: assessing the role of topography and forest interactions. Journal of Hydrology 348, 379–394.

McMichael, C.E., Hope, A.S., 2007. Predicting streamflow response to fire-induced landcover change: Implications of parameter uncertainty in the MIKE SHE model. Journal of Environmental Management 84, 245–256.

McMichael, C.E., Hope, A.S., Roberts, D.A., Anaya, M.R., 2004. Post-fire recovery of leaf area index in California chaparral: a remote sensing-chronosequence approach. International Journal of Remote Sensing 25, 4743–4760.

Plummer, M., 2008. Penalized loss functions for Bayesian model comparison. Biostatistics 9, 523–539.

Qian, S.S., Cuffney, T.F., Alameddine, I., McMahon, G., Reckhow, K.H., 2010. On the application of multilevel modeling in environmental and ecological studies. Ecology 91, 355–361.

Raudenbush, S.W., Bryk, A.S., 2002. Hierarchical linear models: Applications and data analysis methods, 2nd ed. Sage, Thousand Oaks, California.

Sahin, V., Hall, M.J., 1996. The effects of afforestation and deforestation on water yields. Journal of hydrology 178, 293–309.
Scott, D.F., 1993. The hydrological effects of fire in South African mountain catchments. Journal of Hydrology 150, 409–432.
Seo, J.I., Nakamura, F., Nakano, D., Ichiyanagi, H., Chun, K.W., 2008. Factors controlling the fluvial export of large woody debris, and its contribution to organic carbon budgets at watershed scales. Water Resources Research 44.
Shakesby, R.A., Doerr, S.H., 2006. Wildfire as a hydrological and geomorphological agent. Earth Science Reviews 74, 269–307.
Spiegelhalter, D.J., Best, N.G., Carlin, B.P., Linde, A. van der, 2002. Bayesian Measures of Model Complexity and Fit. Journal of the Royal Statistical Society. Series B (Statistical Methodology) 64, 583–639.
Stednick, J.D., 1996. Monitoring the effects of timber harvest on annual water yield. Journal of Hydrology 176, 79–95.
Steele, F.A., 2008. Module 5: Introduction to Multilevel Modelling (Concepts). Centre for Multilevel Modelling, University of Bristol.
Stegmueller, D., 2013. How Many Countries for Multilevel Modeling? A Comparison of Frequentist and Bayesian Approaches. American Journal of Political Science.
Wagner, T., Hayes, D.B., Bremigan, M.T., 2006. Accounting for multilevel data structures in fisheries data using mixed models. Fisheries 31, 180–187.
Webb, A.A., Kathuria, A., 2012. Response of streamflow to afforestation and thinning at Red Hill, Murray Darling Basin, Australia. Journal of Hydrology 412–413, 133–140.
Wehrly, K.E., Brenden, T.O., Wang, L., 2009. A Comparison of Statistical Approaches for Predicting Stream Temperatures Across Heterogeneous Landscapes1. Journal of the American Water Resources Association (JAWRA) 45, 986–997.
Westerling, A.L., Bryant, B.P., 2008. Climate change and wildfire in California. Climatic Change 87, 231–249.
Wilcox, B.P., Owens, M.K., Dugas, W.A., Ueckert, D.N., Hart, C.R., 2006. Shrubs, streamflow, and the paradox of scale. Hydrol. Process. 20, 3245–3259.
Williams, A.A.J., Karoly, D.J., Tapper, N., 2001. The sensitivity of Australian fire danger to climate change. Climatic Change 49, 171–191.
Zhang, L., Dawes, W.R., Walker, G.R., 2001. Response of mean annual evapotranspiration to vegetation changes at catchment scale. Water Resour. Res. 37, 701–708.

Chapter 3: Inter-Seasonal Variability in Baseflow Recession Rates: The Role of Antecedent Storage in Central California Watersheds

Baseflow recession rates vary inter-seasonally in many watersheds. This variability is most commonly associated with seasonal changes in evapotranspiration; however, an additional and less studied control over inter-seasonal baseflow recession rates is the effect of watershed antecedent storage conditions. Understanding the role of antecedent storage on baseflow recession rates is crucial for Mediterranean-climate regions, where seasonal asynchronicity of precipitation and energy levels produces large inter-seasonal differences in watershed storage conditions. The primary objective of this study was to test the effect of antecedent watershed storage on baseflow recession rates in four central California watersheds using antecedent streamflow cumulated over the water year as a surrogate for watershed storage conditions. In addition, a parsimonious storage-discharge model consisting of two nonlinear stores in parallel was developed as a heuristic tool for examining the empirical results and providing insight into the hydrologic processes that govern inter-seasonal variability in baseflow recession rates. Baseflow recession rates and antecedent storage exhibited a negative power-law relation, with baseflow recession rates decreasing by up to an order of magnitude as antecedent storage levels increased. Inference based on the storage-discharge model indicated that the

dominant source of recession flow shifts from small, quickly-recharged aquifers at the beginning of the wet season to large, seasonal aquifers as the wet season progresses. Antecedent storage was determined to be a key control on baseflow recession rates in California watersheds and should be accounted for along with evapotranspiration when characterizing or predicting the inter-seasonal variability of baseflow recession rates.

3.1. Introduction

Baseflow recession rates represent a measure of how baseflow, or the portion of streamflow that derives from aquifers, decreases following a recharge event. They are a function of the discharge magnitude and the discharge recession rate from each watershed aquifer contributing to baseflow. Baseflow recession rates provide insight into the inner workings and storage properties of watershed aquifers (Hall, 1968) and may be used for evaluating the effects of land-cover change on baseflow (Federer, 1973), for quantifying evapotranspiration (ET) rates in a watershed (Szilagyi et al., 2007), low flow prediction (Tague and Grant, 2009), baseflow separation (Eckhardt, 2005) and hydrologic modeling (Tallaksen, 1995).

In many watersheds, the baseflow recession rate for individual recession curves varies throughout the year. This inter-seasonal variability is most commonly associated with fluctuations in ET, with a faster baseflow recession rate corresponding to higher ET (Aksoy and Wittenberg, 2011; Federer, 1973; Shaw and Riha, 2012; Szilagyi et al., 2007; Wang and Cai, 2010; Wittenberg and Sivapalan,

1999). An additional and less studied control over inter-seasonal baseflow recession rates is the effect of watershed antecedent storage conditions (Biswal and Kumar, 2012; Harman et al., 2009; McMillan et al., 2010; Mishra et al., 2003; Shaw et al., 2013). Harman et al. (2009) theorized that in watersheds with multiple aquifers, differences in discharge recession rates between aquifers may lead to a decrease in baseflow recession rate during wet periods, since greater amounts of storage accumulate in aquifers with slower discharge recession rates compared to aquifers with faster discharge recession rates. However, the relation between baseflow recession rates and storage has not been characterized for many environments, including Mediterranean-climate regions (MCRs).

MCRs are water-limited environments that are uniquely characterized by their regime of warm, dry summers and cool, wet winters. While only occupying small parts of Australia, California, Chile, the Mediterranean Basin and South Africa, MCRs are noted for being disproportionally impacted by human development and for having limited local water resources (Rundel, 2004). The seasonal asynchronicity of precipitation and energy levels in MCRs contributes to the development of two different hydrologic regimes within MCR watersheds; an energy-limited winter wet season and a water-limited summer dry season. As storage levels differ between these two periods, baseflow recession rates at the beginning of the wet season may not be the same as those at the end of the wet season.

The effect of increases in wet season storage on baseflow recession rates in MCRs is not well understood. Sayama et al. (2011) observed that baseflow recession

rates were slower at higher levels of total watershed storage than at lower levels of total water storage for two northern California watersheds. However, the relation between baseflow recession rates and antecedent storage has not been quantified and the watershed processes that produce this change have not been investigated. The primary objective of this study was to elucidate the relation between baseflow recession rates and antecedent storage levels in four central California watersheds. To account for the partial contribution of ET on baseflow recession rates, the analysis was limited to periods where actual ET was at a minimum and the expected effect on baseflow recession rates was low. The secondary objective of this study was to develop a parsimonious storage-discharge model for use as a heuristic tool to examine the empirical results and provide insight into the hydrologic processes that govern inter-seasonal variability in baseflow recession rates. This knowledge is important for proper hydrologic modeling of California watersheds.

3.2. Watersheds

The research watersheds are located within the Santa Lucia Mountains along the Central Coast region of California (Figure 7). The Santa Lucia Mountains are characterized by steep topography with peak elevations exceeding 2000m. The mountains are underlain primarily by late-Cenozoic marine sediments with a basement of pre-Cenozoic granite rock from the Salinian Block (Ducea et al., 2003). Most rainfall is generated by frontal systems and spatial variation in rainfall totals is

largely controlled by orographic effects. Vegetation is a mosaic of grasslands, coastal sage scrub, chaparral, oak woodlands, and forests (Callaway and Davis, 1993).

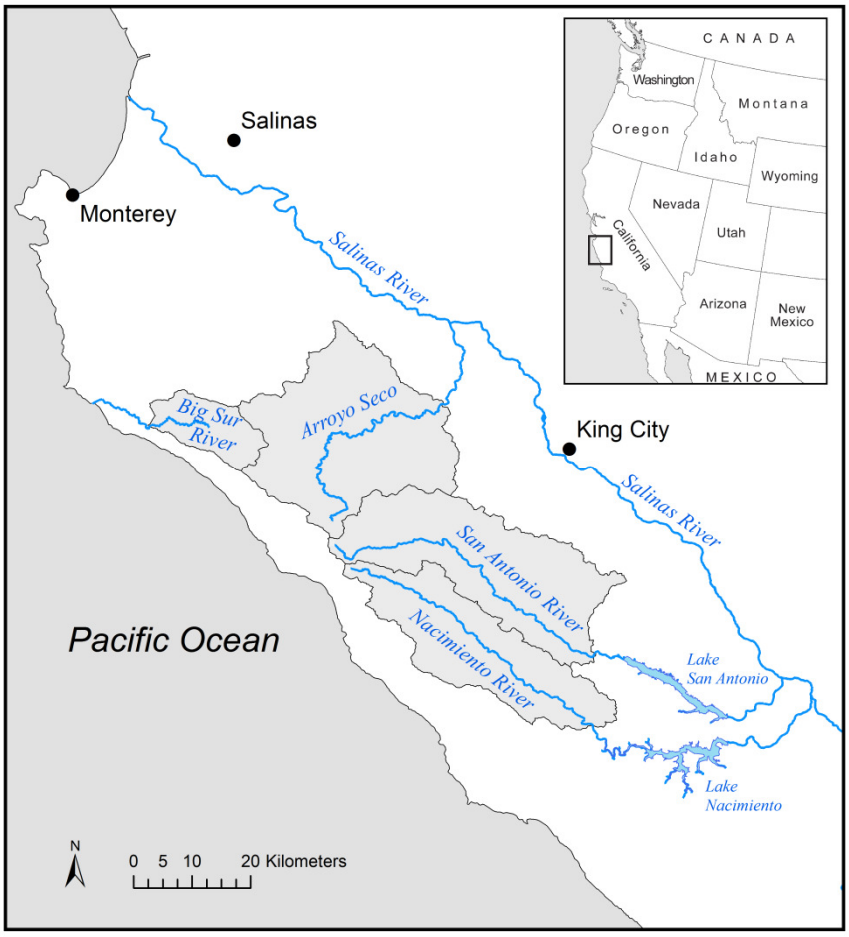

Figure 7: Map of study watersheds.

Four watersheds were found to be suitable for investigation; Arroyo Seco, Big Sur River, Nacimiento River, and San Antonio River (Table 5). These watersheds were selected from US Geological Survey (USGS) streamflow gauges. Big Sur is located on the windward side of the Santa Lucia Mountains and is smaller and wetter than the other three watersheds. Arroyo Seco, Nacimiento, and San Antonio are each

Table 5: Summary of watershed characteristics.

Name	USGS ID	Area (km^2)	MAP (mm)	MAQ (mm)	Zero Flow Days (%)	Geology (% sedimentary)	Mean soil depth (cm)	Soil porosity	Mean slope	Drainage density	Mean LAI	Record Period
Arroyo Seco	11152000	632.0	708	231	12.3	44.0	56	0.46	24.17	0.36	2.44	1943-2011
Big Sur	11143000	119.1	1073	763	0	7.9	53	0.31	29.29	0.35	3.54	1952-2011
Nacimiento	11148900	419.6	568	386	30	85.5	64	0.55	16.97	0.36	2.02	1972-2011
San Antonio	11149900	562.0	587	170	44.8	76.4	81	0.78	15.55	0.40	1.83	1966-2011

MAP: mean annual precipitation; MAQ: mean annual streamflow; LAI: leaf-area index

located on the leeward side of the Santa Lucia Mountains. Chaparral vegetation dominates the higher elevations of these watersheds while woodland and grassland are most prevalent in the lowland areas.

The wet season in central California generally falls within the period of October to April, with large inter-annual variability in precipitation amounts. Figure 8 shows mean monthly precipitation totals (wateryears 1976 to 2005) for the four watersheds. These values were derived from the Parameter-elevation Regressions on Independent Slopes Model (PRISM) product produced by the Climate Group at Oregon State University (http://prism.oregonstate.edu). Watershed mean monthly precipitation totals vary for each of the four watersheds, though seasonal patterns show great similarity. The majority of annual precipitation falls during December, January, February and March. Almost no precipitation occurs during the summer.

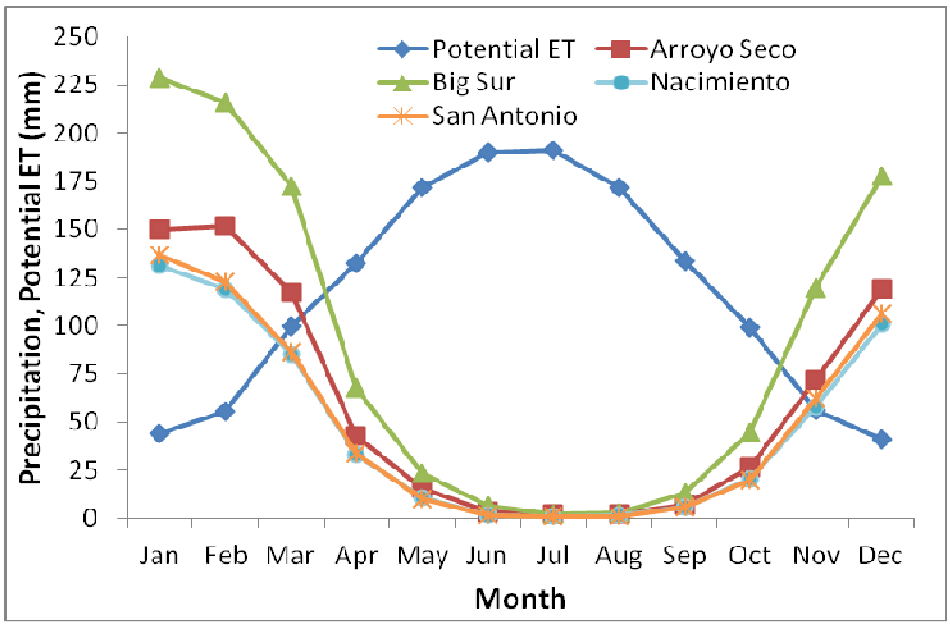

Figure 8: Mean monthly precipitation (1976-2005) for each watershed and mean monthly potential ET (1994-2011).

Potential ET levels from a California Irrigation Management Information System (CIMIS) (www.cimis.water.ca.gov) meteorological station located in the Salinas Valley to the east of the Santa Lucia Mountains are also displayed in Figure 8. Potential ET in central California follows the seasonal energy cycle. Lowest levels occur from November through February and the highest levels in June and July. During the dry period, potential ET exceeds precipitation levels. This extended period of seasonal water-deficit in central California creates very low soil moisture and storage levels at the end of the dry season (Miller et al., 1983). During the winter wet period, precipitation exceeds potential ET, allowing storages to be recharged.

3.3. Conceptual framework for inter-seasonal variability in baseflow recession rates

The hydrologic controls that are expected to produce variability in inter-seasonal baseflow recession rates are the physical properties of watershed aquifers, fluxes to and from an aquifer, and inter-seasonal differences in storage levels between watershed aquifers. In this section, each of these controls is first examined individually and then used collectively to explore how baseflow recession rates may vary throughout the wet season in California watersheds.

3.3.1. Controls on baseflow recession rates

The amount of discharge and discharge recession rate from a single aquifer will vary as a function of storage level and aquifer physical properties such as aquifer size, geometry, porosity, and saturated hydraulic conductivity (Brutsaert and Nieber, 1977). Although the properties of a given aquifer are relatively static, they may vary greatly from aquifer to aquifer and produce a range of discharge characteristics. For a given storage capacity, high initial aquifer discharge magnitudes generally lead to a rapid depletion of storage and a fast aquifer discharge recession rate. Hence, recession rates from small aquifers with high saturated hydraulic conductivities and high hydrological connectivity to the stream (e.g. riparian aquifers) are generally faster than recession rates from larger aquifers that vary over seasonal time-scales and have low saturated hydraulic conductivities and low connectivity to the stream (e.g. hillslopes). In some aquifers, discharge may be threshold-based when connectivity between an aquifer and stream is limited for periods of time (Smakhtin, 2001).

During the recession period, fluxes to and from an aquifer affect storage levels in an aquifer, and thus, the aquifer discharge recession rate. Fluxes to an aquifer during the recession period decrease the discharge recession rate and may occur from soil recharge or when discharge from one aquifer recharges another aquifer. Fluxes from an aquifer during the recession period, excluding discharge to a stream, include ET and losses to other aquifers. The extent to which ET affects storage levels depends on the spatial distribution of vegetation with direct access to aquifers feeding baseflow, which in turn depends on the spatial distribution of shallow groundwater

and/or deep rooted vegetation within a watershed (Tallaksen, 1995). Fluxes from an aquifer increase the discharge recession rate.

In watersheds with more than one aquifer, differences in the relative discharge magnitude from each aquifer may produce variability in baseflow recession rates (Moore, 1997). The source of these differences largely stems from variability in aquifer discharge recession rates, though differences in recharge, aquifer size, and discharge-thresholds may also be factors. Aquifers with fast discharge recession rates have the greatest impact on baseflow during initial periods following a recharge event, but rapid depletion of storage levels supports little sustained discharge. Aquifers with slow discharge recession rates, on the other hand, have a more muted response to recharge events. The slow release of water from these aquifers allows storage to accumulate during extended periods of recharge (Harman et al., 2009), shifting the dominant control on baseflow from aquifers with faster discharge recession rates to aquifers with slower discharge recession rates.

3.3.2. Baseflow recession rates in central California watersheds

At the beginning of the central California wet season, watersheds are characterized by maximum soil moisture and aquifer storage deficits (Miller et al., 1983). Following the first precipitation events of the season, baseflow response is likely to originate from small, low-threshold aquifers that can be quickly recharged and have fast aquifer discharge recession rates. At the same time, channel losses to groundwater may be considerable in many central California watersheds, particularly

for intermittent and ephemeral streams where the water table is disconnected from the stream (Pilgrim et al., 1988). As channel losses increase baseflow recession rates relative to conditions with no channel losses, baseflow recession rates at the beginning of the central California wet season are likely be relatively rapid (Figure 9). The effect of ET on baseflow at the onset of the wet season is likely to be minimal due to low vegetation leaf area combined with low potential ET rates (Figure 8).

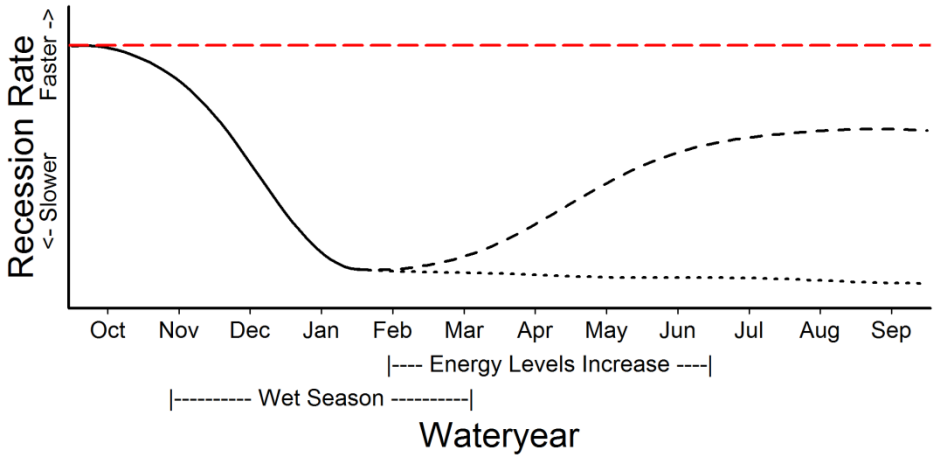

Figure 9: Hypothetical time-series of baseflow recession rates during the central California wateryear.

As the wet season progresses, the primary source of baseflow is expected to shift from aquifers with faster discharge recession rates to aquifers with slower discharge recession rates as the latter aquifers become progressively filled and release larger volumes of water (Harman et al., 2009). These aquifers may also be subject to varying amounts of recharge during the recession period from other aquifers. Channel losses at this time are likely to be negligible in all but the most ephemeral watersheds and/or driest years. Since potential ET levels are at an annual minimum during the

winter period (Figure 8) (Luo et al., 2007), the cumulative effect of these processes should be a continual decrease in baseflow recession rates heading toward the end of the wet season (Figure 9).

Following the wet season, the source of the greatest sustained flows is likely to continually shift to aquifers with slower discharge recession rates as aquifers with faster discharge recession rates become depleted. However, this period coincides with an increase in potential ET levels (Figure 8) and an increase in vegetation leaf area. Two potential effects of ET on baseflow recession rates are illustrated in Figure 9. In the absence of ET from watershed aquifers, the baseflow recession rate would be expected to decrease throughout the summer (Figure 9, dotted line). However, with increasing ET from watershed aquifers, a corresponding increase in baseflow recession rate may be observed (Figure 9, dashed line). The actual effect of ET on dry-season baseflow in central California watersheds requires future study.

3.4. Approach

3.4.1 Derivation of baseflow recession rates

To investigate inter-seasonal changes in baseflow recession rates, baseflow recession rates need to be comparable from one baseflow recession curve to another. Baseflow recession rates along a single baseflow recession curve often vary with baseflow magnitude. In order to account for baseflow magnitude in analyzing rates of baseflow recession, Brutsaert and Nieber (1977) proposed eliminating the time

variable from the baseflow recession curve and comparing the change in baseflow magnitude *dQ/dt* to the observed baseflow *Q*, such that

$$-\frac{dQ}{dt} = f(Q). \tag{9}$$

This relationship is referred to as the recession slope curve (Rupp and Selker, 2006a). The recession slope curve has often been observed to be approximately linear when plotted graphically on a $\log(-dQ/dt) - \log(Q)$ plot, which implies a power-law relation;

$$-\frac{dQ}{dt} = aQ^b \tag{10}$$

where *Q* is baseflow discharge in mm, *t* is time (daily), *a* is the value of *-dQ/dt* when $Q = 1$ and *b* is the slope of the $\log(-dQ/dt) - \log(Q)$ relation (Clark et al., 2009).

When the exponent *b* is equal to one, the recession slope curve simplifies to a linear relation between *-dQ/dt* and *Q*, whereas an exponent other than one indicates a nonlinear relation, or power-law nonlinearity. If the recession slope curve is not linear on a $\log(-dQ/dt) - \log(Q)$ plot, the recession slope curve may be considered to be concave nonlinear (Wang, 2011). *dQ/dt* was computed as the difference between two consecutive points on the recession curve,

$$\frac{dQ}{dt} = \frac{Q_i - Q_{i-1}}{\Delta t}, \tag{11a}$$

while *Q* was computed as the mean of two consecutive recession points;

$$Q = \frac{Q_i + Q_{i-1}}{2}. \quad (11b)$$

Baseflow recession curves were defined as a consecutive decline in the streamflow hydrograph for at least four days following the exclusion of the first two days after a stormflow peak. Each individual recession slope curve was analyzed visually for anomalous reductions in *dQ/dt* that were likely associated with precipitation events that were large enough to reduce the baseflow recession rate but not increase the magnitude of baseflow. These points were removed from the subsequent analysis, though the study results were not sensitive to this criterion.

To isolate the effect of storage differences on baseflow recession rates, the influence of ET on baseflow recession rates must be accounted for or minimized. Only recession curves during the period from November to February were included for examination of inter-seasonal changes. Both potential ET rates (Figure 8) and actual ET rates (Luo et al., 2007) are at their annual minimum during this period.

When the magnitude of baseflow change is smaller than the precision of the stream gauge, the recession slope curve may display discretization errors on a $\log(-dQ/dt) - \log(Q)$ plot (Rupp and Selker, 2006b). This problem is exacerbated in gauge networks such as USGS, where precision for low flows may be very poor (Archfield and Vogel, 2009). Following a recommendation by Rupp and Selker (2006b), the time interval *dt* in Equation 11a was increased for flows below the expected precision of the gauge until the change in baseflow *dQ* exceeded a critical

precision threshold dQ_{crit}. The value of dQ_{crit} for each watershed was determined empirically by visual inspection.

3.4.2. Quantifying antecedent storage

The watersheds in this study are large, non-research watersheds and direct measurements of antecedent storage conditions are not available. Meanwhile, estimates of antecedent storage based on continuous hydrologic models require an a-priori or calibrated estimate of the baseflow recession rate, making modeling approaches unsuitable for estimating antecedent storage in this study. An alternative measure for estimating antecedent storage that does not require a-priori knowledge of baseflow recession rates is cumulative antecedent streamflow for a designated period prior to the baseflow recession curve of interest. Cumulative antecedent streamflow has previously been used by Mishra (2003) to predict inter-seasonal changes in recession rates for the Nile River in Ethiopia. A similar approach was adopted for this study in central California watersheds, with cumulative antecedent streamflow calculated from the beginning of the wateryear (October 1) to the start of each baseflow recession curve. Although cumulative antecedent streamflow cannot account for storage depletion during inter-storm periods, it was assumed that antecedent storage at the beginning of each recession event was a function of wateryear-to-date cumulative antecedent streamflow. The goal with this measure was to provide a first-order approximation of inter-seasonal storage levels in the absence of direct measurements or a continuous hydrologic model.

3.5. Effect of antecedent storage on recession slope curves

All recession curve data between the months of November and February were binned by wateryear-to-date cumulative antecedent streamflow and analyzed collectively on a $\log(-dQ/dt) - \log(Q)$ plot (Figure 10). The six cumulative antecedent streamflow bins (0mm - 25mm, 25mm - 50mm, 50mm - 100mm, 100mm - 200mm, 200mm - 300mm, and 300+mm) were selected to provide an approximately equal distribution of recession curve data across the bins. Despite considerable overlap between the binned recession slope curves, baseflow recession rates for a given baseflow magnitude decreased with higher cumulative antecedent streamflow. This indicates that during periods with low ET, baseflow recession rates in central California watersheds decrease with higher storage levels.

Visual inspection of the recession slope curve for each cumulative antecedent streamflow bin in Figure 10 indicated that the binned recession slope curves were close to linear. Consequently, each binned recession slope curve was modeled using a power-law function (Equation 10). While alternative, more complex models (e.g. Kirchner 2009) may have provided a better fit for some of the recession slope curves, a power law was selected as the most appropriate model for all recession slope curves collectively. A linear least-squares regression on log-transformed values of Q and dQ/dt was found to best characterize the recession slope curves (Xiao et al., 2011).

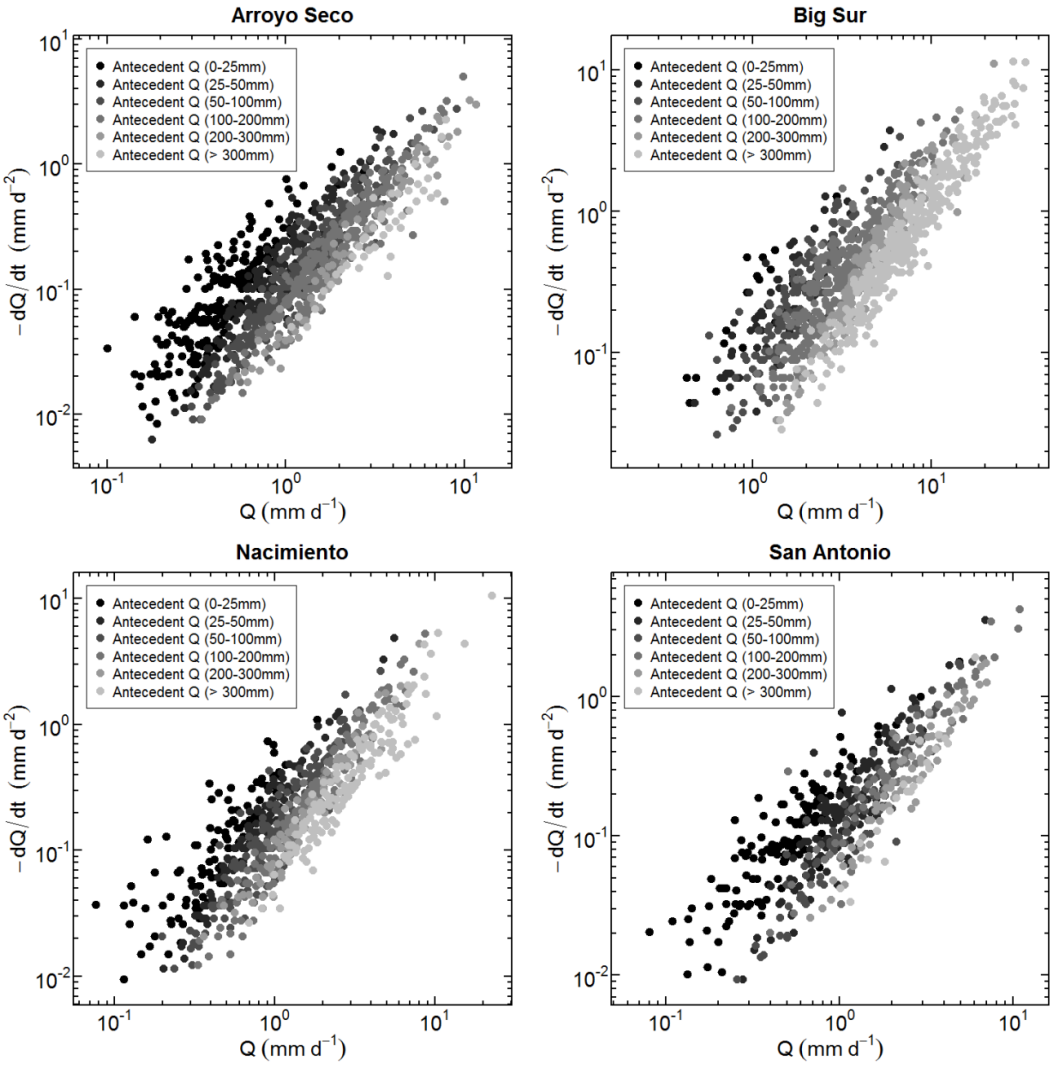

Figure 10: Changes in recession slope curves for different levels of cumulative antecedent streamflow for the period from November to February.

The parameters and coefficient of determination (R^2) for each regression model, as well as dQ_{crit} values for each watershed, are provided in Table 6. The minimum R^2 value was 0.699, while over half of the models had R^2 values greater than 0.9. This suggests that the assumption of a power-law recession slope curve model was likely appropriate. The smallest R^2 value in each of the watersheds was

associated with recession slope curves from the 0 - 25 mm cumulative antecedent streamflow bins. These small R^2 values may be ascribed to heterogeneity in the source of early season baseflow as different combinations of spatially distributed, low-threshold aquifers may be active at the beginning of the wet season (Biswal and Kumar, 2012).

Table 6: Fit of linear regression models on log-transformed data for six wateryear-to-date (WYTD) cumulative antecedent streamflow bins. The refitted model was calculated with *b* fixed at the median *b* value of the original model.

		WYTD cumulative antecedent		Original model			Recomputed model		
Watershed	dQ_{Crit}	streamflow (mm)	*n*	R^2	*a*	*b*	R^2	*a*	Median *b*
Arroyo Seco	0.1	0-25	198	0.712	0.288	1.509	0.693	0.355	1.753
		25-50	169	0.909	0.165	1.808	0.903	0.166	
		50-100	269	0.928	0.101	1.777	0.928	0.102	
		100-200	242	0.912	0.067	1.765	0.912	0.068	
		200-300	79	0.955	0.049	1.741	0.955	0.048	
		300+	45	0.867	0.041	1.633	0.862	0.035	
Big Sur	0.25	0-25	20	0.764	0.208	1.633	0.760	0.210	1.751
		25-50	57	0.775	0.133	1.699	0.762	0.122	
		50-100	141	0.780	0.085	1.793	0.779	0.087	
		100-200	283	0.852	0.052	1.723	0.851	0.050	
		200-300	194	0.932	0.021	1.989	0.919	0.030	
		300+	342	0.935	0.019	1.778	0.934	0.020	
Nacimiento	0.1	0-25	103	0.699	0.322	1.345	0.643	0.448	1.725
		25-50	105	0.958	0.237	1.854	0.953	0.230	
		50-100	135	0.885	0.152	1.698	0.885	0.152	
		100-200	149	0.951	0.097	1.772	0.950	0.099	
		200-300	75	0.939	0.088	1.752	0.938	0.089	
		300+	142	0.901	0.065	1.612	0.897	0.058	
San Antonio	0.12	0-25	136	0.782	0.234	1.259	0.696	0.320	1.677
		25-50	128	0.800	0.134	1.694	0.800	0.134	
		50-100	103	0.901	0.100	1.661	0.901	0.099	
		100-200	61	0.888	0.103	1.472	0.871	0.089	
		200-300	72	0.931	0.058	1.704	0.931	0.059	
		300+	22	0.933	0.035	2.017	0.907	0.048	

The regression model *b* parameters ranged from 1.259 to 2.017, but most were centered between 1.60 and 1.80 (Table 6). These *b* values fell within the range of values reported in the literature (Harman et al., 2009). For each watershed, the values of the *a* parameter generally decreased with increasing cumulative antecedent streamflow levels (Table 6). However, the precise relation between *a* and cumulative antecedent streamflow was difficult to isolate since both *a* and *b* were free parameters. To test the sensitivity of *a* to changes in cumulative antecedent streamflow, the regression model was refitted with *b* fixed at the median value of the six cumulative antecedent streamflow bins in each watershed (Table 6). A linear regression line was then recalculated using log-transformed values of Q and dQ/dt. Despite using a non-optimal slope for each regression model, the R^2 values decreased by less than 0.01 for the majority of the regression models and less than 0.03 for all but two models. This shows that the regression model was relatively insensitive to *b* and that most inter-seasonal variability in recession slope curves was reflected in *a*. This finding is consistent with observations made by Shaw et al. (2013).

The refitted *a* values were plotted against the mean cumulative antecedent streamflow of each cumulative antecedent streamflow bin (Figure 11). Baseflow recession rates and antecedent storage exhibited a negative power-law relation. To characterize this relation, a linear least-squares regression on log-transformed values of *a* and mean cumulative antecedent streamflow was computed and plotted in Figure 11, with the model equations displayed in the legend. The *a* parameter decreased by up to an order of magnitude following initial baseflow events and stabilized when

cumulative antecedent streamflow was greater than 250 mm. This stabilization implied that storages within the watershed were reaching capacity (Sayama et al., 2011). The similarity in the negative power-law relation between cumulative antecedent streamflow and *a* for all four watersheds suggests similar controls over inter-seasonal baseflow recession rates.

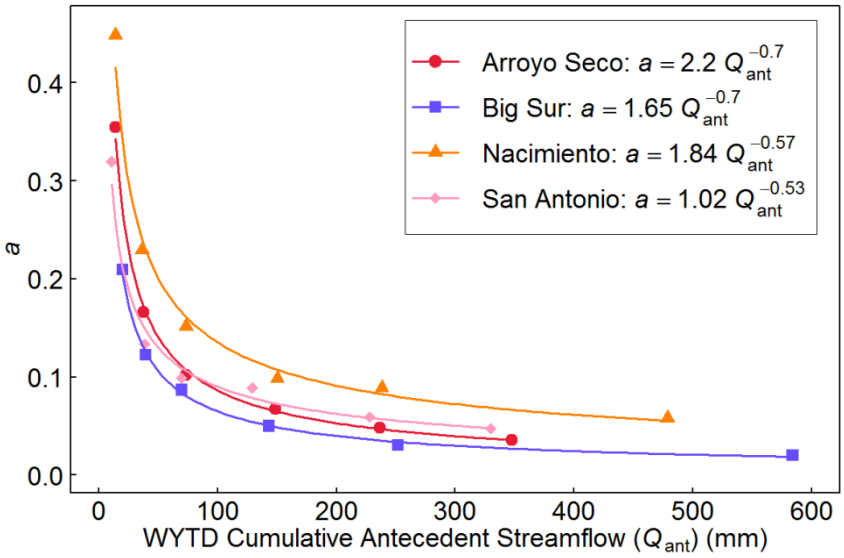

Figure 11: Plot of *a* against wateryear-to-date (WYTD) cumulative antecedent streamflow (Q_{ant}). The power-law regression equation is displayed in the legend.

3.6. Evaluating inter-seasonal variability in baseflow recession rates using a storage-discharge model

The empirical results outlined above indicated that with increasing cumulative antecedent streamflow, baseflow recession rates decreased and recession slope curves maintained characteristics of a power-law function. In order to explore the processes that may have produced these results, a parsimonious storage-discharge model was

developed as a heuristic tool to replicate inter-seasonal variability in baseflow recession rates.

3.6.1. Storage-discharge model

Simple storage-discharge models conceptualize recession flows as originating from a single homogeneous store. A relation linking storage and baseflow can be represented as a power-law function:

$$Q_s = cS^d, \tag{12}$$

where Q_s is discharge from storage, S is aquifer storage in mm, and c ($\mathrm{mm^{1-d}\ t^{-1}}$) and d (-) are defined in terms of a and b from equation 10 (Clark et al., 2009):

$$c = [a(2-b)]^{1/(2-b)} \tag{13a}$$

$$d = 1/(2-b). \tag{13b}$$

The storage-discharge relation in equation 12 reduces to a linear reservoir when d is equal to one. The continuity equation for a single store during a recession period may be represented as

$$-\frac{dS}{dt} = Q_s, \tag{14}$$

with the assumption that fluxes to storage (e.g. recharge) and from storage (e.g. ET, discharge to other stores) are negligible during the recession period.

The behavior of a single store model with no additional fluxes besides discharge to a stream is invariant, and consequently, inadequate for replicating inter-seasonality of baseflow recession rates (McMillan et al., 2010; Sloan, 2000). Inter-seasonality implies different controls on recession flows at different times of the year. The effect of multiple stores configured in parallel may be represented by

$$Q = \sum_j^J Q_{sj} \tag{15}$$

where Q is baseflow at the streamflow gauge, Q_{sj} is discharge to the stream from the jth store, and J is the total number of stores.

For this study, a parsimonious storage-discharge model consisting of two nonlinear stores in parallel was selected to isolate the role of storage on baseflow recession rates. Conceptually, the faster of the two stores was considered to represent low-threshold aquifers that were responsive throughout the wet season and had high hydrological connectivity to the stream and fast discharge recession rates (e.g. shallow riparian aquifers). The slower of the two stores was considered to represent seasonal aquifers located further up hillslopes with lower saturated hydraulic conductivity and slower discharge recession rates. It was assumed that only the fast store was active at the beginning of the wet season since the contribution from aquifers with slow discharge recession rates is likely to be negligible due to low storage levels. By the end of the wet season, both the fast and slow stores were assumed to contribute to recession flows. The details of the steps used to calibrate parameters c, d, and the

maximum size of active storage (herein referred to as S_{max}) for both model stores are provided in Appendix A.

3.6.2 Model results

The fit of the modeled recession slope curve to the observed recession slope curve for the lowest and highest cumulative antecedent streamflow bins is shown in Figure 12. Under low cumulative antecedent streamflow conditions when only a single power-law store was active, the modeled recession slope curve plotted as a linear line on a $\log(-dQ/dt) - \log(Q)$ plot and closely matched the observed recession slope curve. Similarly, at high cumulative antecedent streamflow levels, when both power-law stores were active, the modeled recession slope curve also maintained characteristics of a power-law function, but at a slower rate of recession. Power-law behavior was maintained in the latter case, even though both stores were active, because discharge from the slow store was much larger than discharge from the fast store, such that the modeled recession slope curve approximated the power-law behavior of the slow store. At high cumulative antecedent streamflow levels, the influence of the fast store, if observable, was small and short-lived. An example of this influence was observed in Arroyo Seco, where the modeled recession slope curve becomes concave upwards for high magnitude flows, reflecting the brief influence of fast-store discharge on baseflow when storage levels were high.

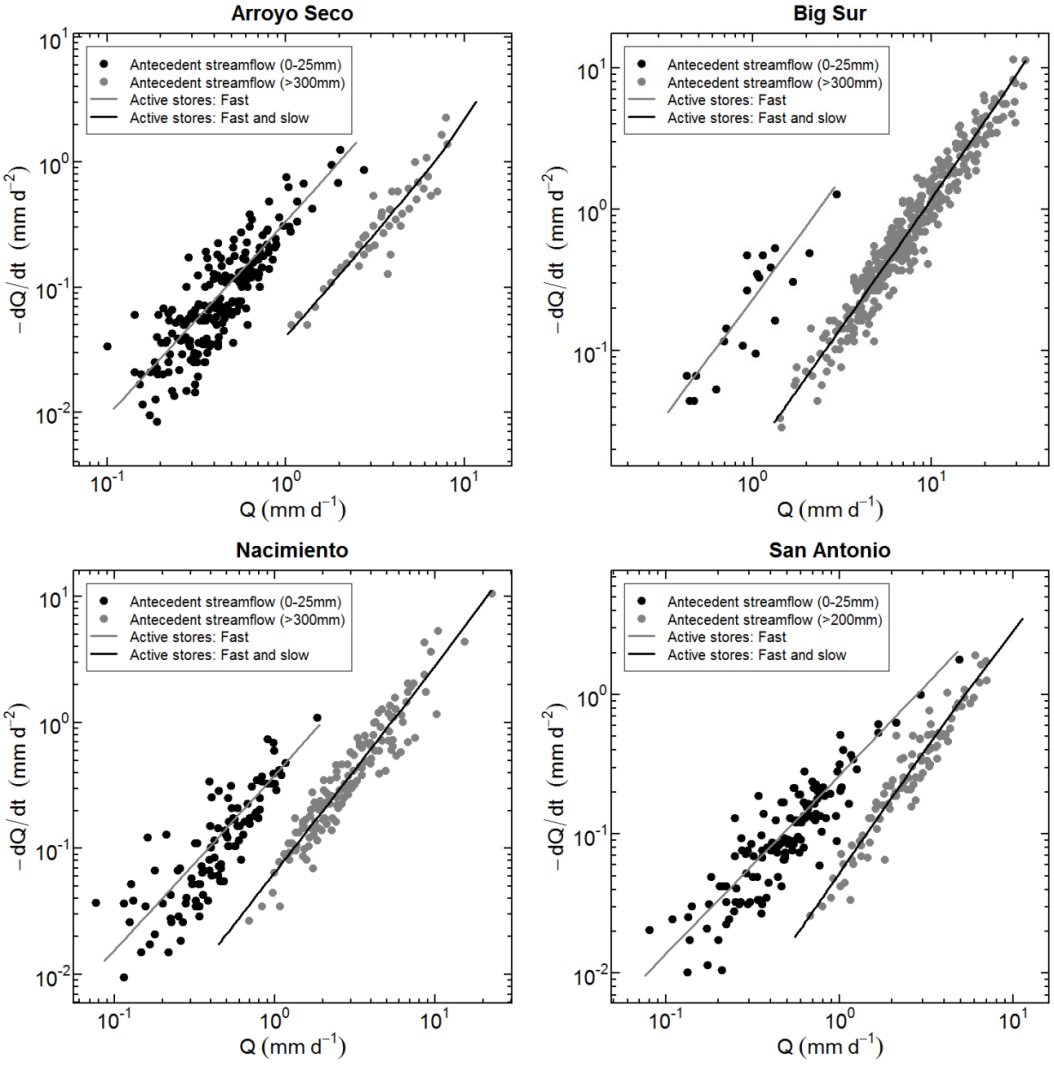

Figure 12: Fit of the storage-discharge model with two stores in parallel to recession slope curves of the lowest and highest cumulative antecedent streamflow bins. Under low cumulative antecedent streamflow conditions, the fast store was assumed to be initially full and the slow store initially empty. Under high cumulative antecedent streamflow conditions, both stores were assumed to be initially full.

The modeled store characteristics are displayed in Table 7. To facilitate direct comparisons of baseflow recession rates between the fast and slow store, the baseflow recession rate *dQ/dt* was calculated at two fixed baseflow magnitudes *Q*, 2 mm and

0.5 mm (Table 7). The baseflow recession rate of the slow store ranged from 3.4 to 9.7 times slower than the fast store at 2 mm of baseflow and from 6.0 to 11.2 times slower than the fast store at 0.5 mm of baseflow. In all watersheds, the difference in baseflow recession rate between the fast and slow store increased with decreasing baseflow magnitude. Baseflow recession rates for the slow stores mirrored the percentage of zero flow days in a watershed, with the slowest rate occurring in the perennial watershed Big Sur and the fastest rates occurring in Nacimiento and San Antonio, which are dry for 30% and 44.8% of the year, respectively (Tables 5 and 7). The maximum active storage size S_{max} ranged from 8 to 21 mm for the fast stores and from 134 to 521 mm for the slow stores (Table 7). This corresponded to a slow store capacity that is 6.4 to 24.8 times larger than the fast store. These storage values appear physically plausible, as the aquifers in these watersheds are likely localized in small areas (e.g. riparian zones) and actual aquifer depths are likely much deeper.

Table 7: Simulated store characteristics.

Name	Store	WYTD cumulative antecedent streamflow (mm)	*c*	*d*	S_{max} (mm)	*dQ/dt* at *Q*=2mm	*dQ/dt* at *Q*=0.5mm
Arroyo Seco	Fast	0-25	1.86E-02	2.04	12	0.824	0.102
	Slow	300+	9.81E-06	2.73	159	0.124	0.013
Big Sur	Fast	0-25	9.13E-04	2.72	21	0.643	0.067
	Slow	300+	2.00E-11	4.51	521	0.066	0.006
Nacimiento	Fast	0-25	9.29E-02	1.53	8	0.823	0.127
	Slow	300+	6.88E-05	2.58	145	0.192	0.021
San Antonio	Fast	0-25	9.37E-02	1.35	21	0.559	0.098
	Slow	200+	1.56E-08	4.07	134	0.166	0.015

WYTD: Wateryear-to-date

The storage-discharge model with two stores in parallel replicated both the power-law characteristics of the recession slope curve under low cumulative antecedent streamflow conditions when the fast store was the dominant control on baseflow and under high cumulative antecedent streamflow conditions when the slow store was the dominant control on baseflow (Figure 12). However, as the wet season progressed, the controls on the recession slope curve could be expected to transition between these two end-member conditions. The simulated transition of the recession slope curve from a dominant fast store to a dominant slow store is demonstrated for the Arroyo Seco watershed (Figure 13). The initial storage value (herein referred to as S_o) of the fast store was assumed to equal S_{max} (12 mm) for each of the curves generated, while S_o of the slow store was varied from empty (0 mm) to S_{max} (159 mm). While the recession slope curve displayed power-law characteristics when the slow store was either empty or full, the transition between these two levels introduced concave nonlinearity in the recession slope curve. This concave nonlinearity occurred when discharge from the fast and slow stores were similar in magnitude. The recession slope curves observed in Figure 10 had suggested that the recession slope curve maintains power-law behavior at all levels of cumulative antecedent streamflow. This discrepancy between the empirical results and the modeled results may be due to inadequacies in the storage-discharge model structure. However, it may also reflect imprecision in empirically characterizing the recession slope curves. The degree of concave nonlinearity in the theoretical recession slope curves of Figure 13 is small compared to the observed scatter in the recession slope curves of Figure

10. Further, over short domains, the recession slope curve may appear as a power law (e.g. slow store S_0 = 40 mm).

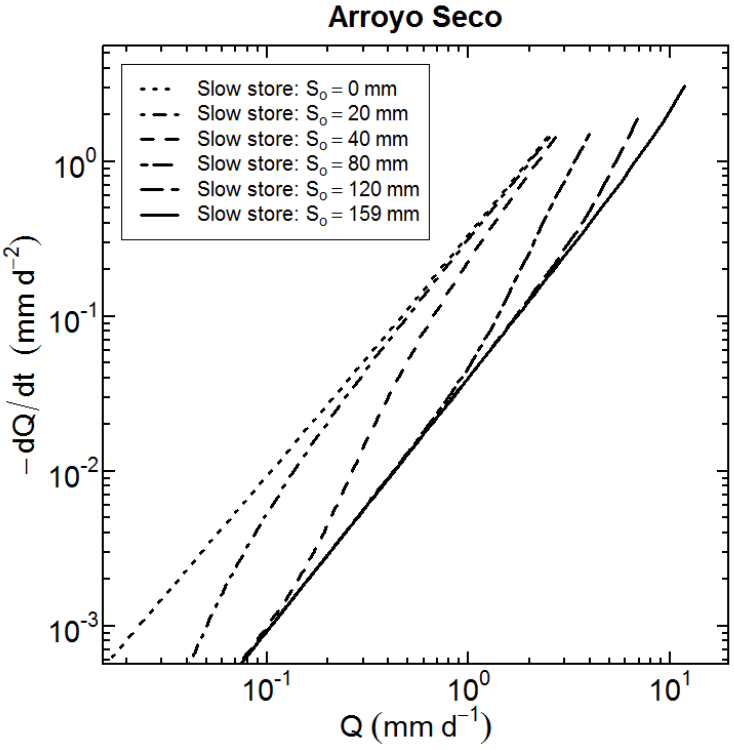

Figure 13: Simulation of the recession slope curve transition from a dominant fast store to a dominant slow store for Arroyo Seco using a storage-discharge model with two stores in parallel. Initial storage S_o of the fast store was fixed at S_{max}, while S_o of the slow store was varied between 0 mm (empty) and 159 mm (full).

In addition to concave nonlinearity, recession slope curves transitioning from a dominant fast store to a dominant slow store have a steeper slope (i.e. larger *b* value) than either of the two end-member recession slope curves (Figure 13). A reexamination of the calculated *b* parameters in Table 6 showed that in two

watersheds, Arroyo Seco and Nacimiento, *b* is higher for the intermediate cumulative antecedent streamflow bins compared to the lowest and highest bins. This behavior is not observed in Big Sur or San Antonio. This suggests that in some watersheds, a model structure with two stores in parallel may provide a good representation of inter-seasonal recession slope curve variability under all wetness conditions, not just the extremes.

3.7. Synthesis

This study investigated the effects of inter-seasonal changes in antecedent storage on baseflow recession rates in four central California watersheds. Using wateryear-to-date cumulative antecedent streamflow as a surrogate measure of storage conditions, baseflow recession rates were observed to decrease by up to an order of magnitude with increasing levels of cumulative antecedent streamflow. Baseflow recession rates and cumulative antecedent streamflow displayed a negative power-law relation, with a rapid decrease in baseflow recession rate following initial baseflow-producing events and subsequent stabilization as watershed storages became full.

Inter-seasonal decreases in baseflow recession rates were well-represented by a storage-discharge model with two nonlinear stores in parallel. The model showed that at the beginning of the central California wet season, the baseflow recession curve could be replicated by a small, fast store. Physically, this store likely corresponds to shallow, quickly-recharged riparian aquifers with high hydrological connectivity to the stream, allowing for rapid responses following precipitation

events. As the wet season progresses, a much larger and much slower store, which is initially empty at the onset of the wet season, is recharged. This slow store, which represents seasonal aquifers within the watershed, becomes the dominant control on baseflow as discharge from the slow store eventually overwhelms discharge from the fast store.

The results of this study have clearly shown that accounting for inter-seasonal differences in storage conditions is important for properly characterizing baseflow recession rates, particularly in MCRs that are typified by large inter-seasonal differences in watershed storage levels. Previous studies of inter-seasonal baseflow recession rate changes in MCRs have focused solely on the role of ET on baseflow recession rates (Aksoy and Wittenberg, 2011; Wittenberg and Sivapalan, 1999). Future work on inter-seasonal variability in MCRs needs to address the relative role of both storage and ET on baseflow recession rates. Further, the effect of other storage-discharge related processes such as channel losses and storage losses also need to be examined.

Finally, there has been recognition in recent years that the controls on recession flows in many watersheds are dynamic (Biswal and Kumar, 2012; McMillan et al., 2010; Mishra et al., 2003; Shaw et al., 2013; Wang and Cai, 2009). This study adds to this understanding by demonstrating how changes in storage can be used to explain inter-seasonality of baseflow recession rates in central California watersheds. This study also demonstrates that the frequent assumption of a single storage-discharge relation for representing baseflow may not be appropriate in some

watersheds, which has implications for hydrologic applications ranging from baseflow separation (Eckhardt, 2005) to rainfall-runoff modeling (Jakeman and Hornberger, 1993).

3.8. Appendix

To evaluate inter-seasonal changes in baseflow recession rates using a storage-discharge model with two stores in parallel, parameters c, d, and the maximum size of active storage S_{max} needed to be calibrated for both the fast and slow model store (Equation 12). The parameters of the fast store were identified by fitting a power-law function to the recession slope curve of the lowest cumulative antecedent streamflow bin (0 - 25mm) in each watershed and using equations 13a and 13b to derive c and d, respectively. S_{max} for the fast store was calculated by inverting equation 12 and assuming that the maximum observed baseflow value (herein referred to as Q_{max}) for the lowest cumulative antecedent streamflow bin corresponded to discharge from the maximum active storage size, S_{max}.

During periods of high cumulative antecedent streamflow, both the fast and slow stores were assumed to be active. Discharge from the slow store was simulated simultaneously with discharge from the fast store and the combined flow was evaluated against the regression-derived recession slope curve of the highest cumulative antecedent streamflow bin using the root mean square error (RMSE) on logged variables. A slow store value of c was selected via a grid search of the probable parameter space. The d parameter of the slow store was then derived from

the *b* parameter of the modeled recession slope curve from the highest cumulative antecedent streamflow bin. S_{max} for the slow store was calculated by deriving Q_{max} for the slow store, which was assumed to be the difference between the maximum observed recession flow value produced in the watershed and Q_{max} of the fast store. This value, along with the *c* and *d* parameters, were used to derive S_{max} of the slow store using equation 12. The recession slope curve for the highest cumulative antecedent streamflow bin was then simulated with the two-store model under the assumption that initial storage for both the fast and slow store was at S_{max}.

The highest cumulative antecedent streamflow bin was used to establish slow-store parameters for all watersheds except San Antonio, which had a *b* value of 2.017 for the highest cumulative antecedent streamflow bin (Table 6). Values greater than 2 translate into negative *d* values, producing a store where discharge magnitude increases with decreasing storage levels. As this parameter value is not physically sound and is inconsistent with *b* values from the other bins, the value was assumed to be an outlier, possibly due to too few data points (N=22) in the development of the regression model. The model parameters for San Antonio were instead obtained from a regression line fitted to all recession data with more than 200mm of wateryear-to-date cumulative antecedent streamflow.

3.9. References

Aksoy, H., Wittenberg, H., 2011. Nonlinear baseflow recession analysis in watersheds with intermittent streamflow. Hydrol. Sci. J. 56, 226–237.

Archfield, S.A., Vogel, R.M., 2009. The Implications of Discretizing Continuous Random Variables: An Example Using the U.S. Geological Survey Reporting Standards for Streamflow Data, in: Proceedings of the American Society of Civil Engineers World Environmental and Water Resources Congress. Kansas City, Missouri.

Biswal, B., Kumar, D.N., 2012. Study of dynamic behaviour of recession curves. Hydrol. Process. In-press, doi: 10.1002/hyp.9604.

Brutsaert, W., Nieber, J.L., 1977. Regionalized drought flow hydrographs from a mature glaciated plateau. Water Resour. Res. 13, 637–643.

Callaway, R.M., Davis, F.W., 1993. Vegetation Dynamics, Fire, and the Physical Environment in Coastal Central California. Ecology 74, 1567–1578.

Clark, M.P., Rupp, D.E., Woods, R.A., Tromp-van Meerveld, H.J., Peters, N.E., Freer, J.E., 2009. Consistency between hydrological models and field observations: linking processes at the hillslope scale to hydrological responses at the watershed scale. Hydrol. Process. 23, 311–319.

Ducea, M., House, M.A., Kidder, S., 2003. Late Cenozoic denudation and uplift rates in the Santa Lucia Mountains, California. Geology 31, 139–142.

Eckhardt, K., 2005. How to construct recursive digital filters for baseflow separation. Hydrol. Process. 19, 507–515.

Federer, C.A., 1973. Forest transpiration greatly speeds streamflow recession. Water Resour. Res. 9, 1599–1604.

Hall, F.R., 1968. Base-flow recessions–a review. Water Resour. Res. 4, 973–983.

Harman, C.J., Sivapalan, M., Kumar, P., 2009. Power law catchment-scale recessions arising from heterogeneous linear small-scale dynamics. Water Resour. Res. 45, W09404.

Jakeman, A.J., Hornberger, G.M., 1993. How much complexity is warranted in a rainfall-runoff model? Water Resour. Res. 29, 2637–2650.

Kirchner, J.W., 2009. Catchments as simple dynamical systems: Catchment characterization, rainfall-runoff modeling, and doing hydrology backward. Water Resour. Res. 45, W02429.

Luo, H., Oechel, W.C., Hastings, S.J., Zulueta, R., Qian, Y., Kwon, H., 2007. Mature semiarid chaparral ecosystems can be a significant sink for atmospheric carbon dioxide. Glob. Change Biol. 13, 386–396.

McMillan, H., Clark, M., Woods, R., Duncan, M., 2010. Improving Perceptual and Conceptual Hydrological Models using Data from Small Basins, in: Status and Perspectives of Hydrology in Small Basins. IAHS Publ. 336-08, pp. 1–6.

Miller, P.C., Poole, D.K., Miller, P.M., 1983. The influence of annual precipitation, topography, and vegetative cover on soil moisture and summer drought in Southern California. Oecologia 56, 385–391.

Mishra, A., Hata, T., Abdelhadi, A.W., Tada, A., Tanakamaru, H., 2003. Recession flow analysis of the Blue Nile River. Hydrol. Process. 17, 2825–2835.

Moore, R.D., 1997. Storage-outflow modelling of streamflow recessions, with application to a shallow-soil forested catchment. J. Hydrol. 198, 260–270.

Pilgrim, D.H., Chapman, T.G., Doran, D.G., 1988. Problems of rainfall-runoff modelling in arid and semiarid regions. Hydrol. Sci. J. 33, 379–400.

Rundel, P.W., 2004. Mediterranean-climate ecosystems: defining their extent and community dominance, in: Arianoutsou, Papanastasis (Eds.), Proceedings 10th MEDECOS Conference, Proceedings 10th MEDECOS Conference. Presented at the 10th MEDECOS Conference, Rhodes, Greece, pp. 1–12.

Rupp, D.E., Selker, J.S., 2006a. On the use of the Boussinesq equation for interpreting recession hydrographs from sloping aquifers. Water Resour. Res. 42, W12421.

Rupp, D.E., Selker, J.S., 2006b. Information, artifacts, and noise in dQ/dt - Q recession analysis. Adv. Water Resour. 29, 154–160.

Sayama, T., McDonnell, J.J., Dhakal, A., Sullivan, K., 2011. How much water can a watershed store? Hydrol. Process. 25, 3899–3908.

Shaw, S.B., McHardy, T.M., Riha, S.J., 2013. Evaluating the influence of watershed moisture storage on variations in baseflow recession rates during prolonged rain-free periods in medium-sized catchments in New York and Illinois, USA. Water Resour. Res. 49, 6022–6028.

Shaw, S.B., Riha, S.J., 2012. Examining individual recession events instead of a data cloud: Using a modified interpretation of dQ/dt–Q streamflow recession in glaciated watersheds to better inform models of low flow. J. Hydrol. 434–435, 46–54.

Sloan, W.T., 2000. A physics-based function for modeling transient groundwater discharge at the watershed scale. Water Resour. Res. 36, 225–241.

Smakhtin, V.U., 2001. Low flow hydrology: a review. J. Hydrol. 240, 147–186.

Szilagyi, J., Gribovszki, Z., Kalicz, P., 2007. Estimation of catchment-scale evapotranspiration from baseflow recession data: Numerical model and practical application results. J. Hydrol. 336, 206–217.

Tague, C., Grant, G.E., 2009. Groundwater dynamics mediate low-flow response to global warming in snow-dominated alpine regions. Water Resour. Res. 45, W07421.

Tallaksen, L.M., 1995. A review of baseflow recession analysis. J. Hydrol. 165, 349–370.

Wang, D., 2011. On the base flow recession at the Panola Mountain Research Watershed, Georgia, United States. Water Resour. Res. 47, W03527.

Wang, D., Cai, X., 2009. Detecting human interferences to low flows through base flow recession analysis. Water Resour. Res. 45, W07426.
Wang, D., Cai, X., 2010. Recession slope curve analysis under human interferences. Adv. Water Resour. 33, 1053–1061.
Wittenberg, H., Sivapalan, M., 1999. Watershed groundwater balance estimation using streamflow recession analysis and baseflow separation. J. Hydrol. 219, 20–33.
Xiao, X., White, E.P., Hooten, M.B., Durham, S.L., 2011. On the use of log-transformation vs. nonlinear regression for analyzing biological power laws. Ecology 92, 1887–1894.

Chapter 4: The Impact of Wildfire on Baseflow Recession Rates in California Watersheds

The effect of wildfire on peak streamflow and annual water yield has been investigated empirically in numerous studies. The effect of wildfire on baseflow recession rates, in contrast, is not well documented. The primary objective of this paper was to examine the effect of wildfire on baseflow recession rates in California at both watershed and regional scales. In addition, inter-seasonal differences in two additional variables, antecedent storage and potential evapotranspiration (ET), were also investigated for their effect on baseflow recession rates and post-fire baseflow recession rate response. A mixed model, which allows for the analysis of data containing an embedded hierarchical structure, was used to statistically model the differences between pre- and post-fire baseflow recession rates. At the regional scale, antecedent storage, potential ET and wildfire were each found to be significant controls on baseflow recession rates. Following fire, baseflow recession rates decreased 52.5% (37.6% to 66.0%), implying that the dominant hydrologic control on post-fire baseflow recession rates are related to post-fire reductions in above-ground vegetation (e.g. decreased interception, decreased soil ET, decreased groundwater ET). Baseflow recession rate response to fire was not sensitive to inter-seasonal differences in antecedent storage or potential ET; however more data will be needed

to conclusively assess this latter result due to weak statistical power for evaluating the interaction variables.

4.1. Introduction

Mediterranean-climate regions (MCRs) are water-limited environments whose water resources are heavily exploited for urban and agricultural uses (Rundel, 2004). Located in parts of Australia, California, Chile, the Mediterranean Basin and South Africa, these regions are distinguished by their climate regime of warm, dry summers and cool, wet winters. The signature vegetation type of MCRs is sclerophyllous shrublands that are subject to regular transformation by wildfire (Rundel, 2004). Wildfire may alter the landscape through the elimination of above-ground vegetation and an increase in hydrophobicity in the soil. These modifications, in turn, may affect watershed hydrology through a reduction in watershed transpirational capacity and a decrease in soil infiltration, respectively.

Post-fire changes in soil hydrophobicity and above-ground vegetation in MCRs have been shown to increase peak flows that produce flooding and debris flows (Cannon et al., 2008; Keller et al., 1997; Wells, 1987) and increase annual flows that that are important for local water supplies (McMichael and Hope, 2007). The effect of wildfire on baseflow, however, is not as well documented. Baseflow represents the portion of streamflow that discharges from groundwater and sustains streamflow between precipitation events. Baseflow is commonly characterized in two ways, by baseflow volume or by baseflow recession rate. Baseflow recession rates

represent the rate of decrease in baseflow volume following a recharge event and are a key tool for low flow prediction (Tague and Grant, 2009) and hydrologic modeling (Tallaksen, 1995).

The effect of wildfire on baseflow in MCRs has primarily been examined during the summer dry period when potential evapotranspiration (ET) is high and recharge to storage is negligible. Baseflow volumes during this period have been shown to increase following wildfire (Colman, 1951; Crouse, 1961; Kinoshita and Hogue, 2011) while post-fire baseflow recession rates have been shown to decrease following the last storms of the wet season (Crouse, 1961; Meixner and Wohlgemuth, 2003). Less is understood about how wildfire affects baseflow during the wet season, when potential ET is lower and storage conditions are more variable. Jung et al. (2009) found that baseflow response to wildfire during the wet season was variable in two adjacent southern California watersheds, with post-fire baseflow volume increasing in one watershed but not the other. No known studies have examined the impact of wildfire on baseflow recession rates during the MCR wet season.

Baseflow recession rates in MCRs have been shown to vary inter-seasonally with changes in antecedent storage and potential ET. In Chapter 3, slower baseflow recession rates were associated with higher levels of antecedent storage in California watersheds. Meanwhile, Wittenberg and Sivapalan (1999) and Aksoy and Wittenberg (2011) reported that slower baseflow recession rates were associated with lower potential ET levels for MCR watersheds in Australia and Turkey. The effect of these inter-seasonal controls on baseflow recession rate response to wildfire is unclear.

The primary objective of this study was to examine the effect of wildfire on baseflow recession rates in California at both watershed and regional scales. Differences between pre- and post-fire baseflow recession rates were modeled statistically using a mixed model (Hox, 2010; Raudenbush and Bryk, 2002). Mixed modeling is a technique that is similar to multiple regression but allows for the analysis of data containing a hierarchical structure (Bickel, 2007). Hierarchical structures occur when data are organized at more than one level, such as when baseflow recession rates are grouped by year. The secondary objective of this study was to investigate how antecedent storage and potential evapotranspiration may both affect baseflow recession rates and affect baseflow recession rate response to wildfire.

4.2. The effect of wildfire on groundwater fluxes

Groundwater discharge to a stream Q_{GW} varies as a function of groundwater storage S_{GW};

$$Q_{GW} = f(S_{GW}). \tag{16}$$

When discharge is the only flux from groundwater storage, the rate at which Q_{GW} decreases over time, or the groundwater discharge recession rate, depends primarily on static physical properties of groundwater storage such as size, geometry, porosity, and saturated hydraulic conductivity (Brutsaert and Nieber, 1977). Groundwater

storage is frequently affected by additional fluxes besides Q_{GW} (Figure 14). These fluxes may include ET directly from groundwater ET_{GW} and recharge to groundwater R_{GW}, such that

$$\Delta S_{GW} = f(ET_{GW}, R_{GW}, Q_{GW}). \quad (17)$$

Fluxes operating concurrently (i.e. during the recession period) with Q_{GW} alter the rate of groundwater storage depletion and thus, the groundwater discharge recession rate. Baseflow recession rates are a function of the groundwater discharge recession rate from each groundwater aquifer contributing to baseflow. For watersheds with a single groundwater aquifer, the groundwater discharge recession rate is equal to the baseflow recession rate.

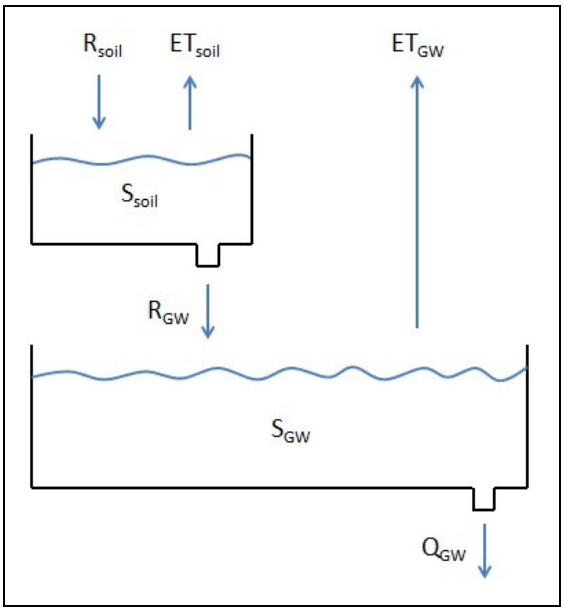

Figure 14: Diagrammatic representation of fluxes to and from groundwater.

Wildfire directly decreases ET from groundwater by reducing above-ground vegetation with access to the watertable and/or the capillary fringe (i.e. phreatophytes) (Figure 14). Phreatophytes are located predominately in and around riparian zones where the watertable is shallow. Changes in ET from groundwater are likely to be most sensitive to burning within this zone. Riparian zones, however, may have lower burn severities and longer fire-return intervals than adjacent upland areas (Luce et al., 2012). Consequently, the effect of decreases in post-fire groundwater ET on baseflow recession rates may vary from event to event depending of the location and severity of the fire. This effect may also vary seasonally; increasing when potential ET levels are highest. The duration of changes in post-fire groundwater ET may range from years to decades depending on the rate of post-fire vegetation recovery.

Wildfire affects recharge to groundwater during the recession period by increasing or decreasing soil moisture levels in the rooting zone above the water table (Figure 14). Elevated soil moisture may occur when post-fire reductions in above-ground vegetation decrease transpiration from the soil matrix (Silberstein et al., 2013). Elevated soil moisture levels may also occur when decreased interception causes an increase in soil infiltration during storm events. Soil hydrophobicity, in contrast, may lower post-fire soil moisture levels by decreasing recharge to groundwater during storm events. Hydrophobicity forms from the heating of soil organic matter during a wildfire and at the plot scale, decreases soil infiltration (Doerr et al., 2000). However at larger scales, spatial heterogeneity in post-fire hydrophobicity may diminish its effect on infiltration (DeBano, 2000; Imeson et al.,

1992). The temporal effects of hydrophobicity may range from months to years, depending on levels of hydrophobicity in the watershed, time elapsed since the fire and post-fire meteorological conditions (Shakesby and Doerr, 2006).

The overall effect of wildfire on baseflow recession rates depends on the net change in post-fire water flux to and from groundwater during the recession period. An increase in net flux to groundwater during the recession period (i.e. slower groundwater depletion rate) decreases baseflow recession rates and implies that processes related to post-fire reductions in above-ground vegetation (e.g. decreased interception, decreased soil ET, decreased groundwater ET) are the dominant hydrologic control on baseflow recession rates. Alternatively, a decrease in net flux to groundwater during the recession period (i.e. faster groundwater depletion rate) increases baseflow recession rates and implies that processes related to hydrophobicity are the dominant hydrologic control on baseflow recession rates.

4.3. Watersheds and data

Watersheds in this study were selected from US Geological Survey (USGS) streamflow network gauges in southern and central California. Watersheds were evaluated for inclusion based on absence of major diversions or regulations (e.g. dams), lack of persistent winter snow cover, limited (less than 5%) urbanization or agriculture, data quality, and having no additional large fires (greater than 5% of watershed area) during the pre- and post-fire periods. Wildfire history for each watershed was obtained from the Fire and Resource Assessment Program (FRAP)

(http://frap.fire.ca.gov). Daily streamflow data were acquired from the USGS (waterdata.usgs.gov). Daily precipitation totals were generated by merging two gridded precipitation data products; the monthly, 2.5 arcminute Precipitation-Elevation Regressions on Independent Slopes Model (PRISM) produced at Oregon State University (http://prism.oregonstate.edu) and the daily, 15 arcminute US Unified Precipitation dataset provided by the National Oceanic and Atmospheric Administration (NOAA) Climate Prediction Center (http://www.esrl.noaa.gov/psd) (Hope et al., 2008). Daily gridded temperature data was obtained from the NOAA Climate Prediction Center (ftp://ftp.cpc.ncep.noaa.gov/precip/daily_grids). Watershed characteristics were attained from the Geospatial Attributes of Gages for Evaluating Streamflow (GAGES-II) database (Falcone, 2011).

Eight watersheds were selected for analysis. A map and description of the watersheds is given in Figure 15 and Table 8, respectively. The watersheds are located along the Coast Range of central California and the Transverse Range of southern California. The watersheds are characterized by steep topography with peak elevations near 2000m asl. The wet season extends from late fall (November) to early spring (April) and is dominated by cyclonic frontal systems approaching from the Pacific Ocean. Annual precipitation in the watersheds ranges from a little more than 600mm to over 1100mm. Annual streamflow is more variable, ranging from 120mm to over 750mm. During the summer dry season, flow ceases in many of the watersheds. The primary vegetation in most of the watersheds is chaparral, with

grasslands, coastal sage scrub, oak woodlands, and forests also being common (Callaway and Davis, 1993).

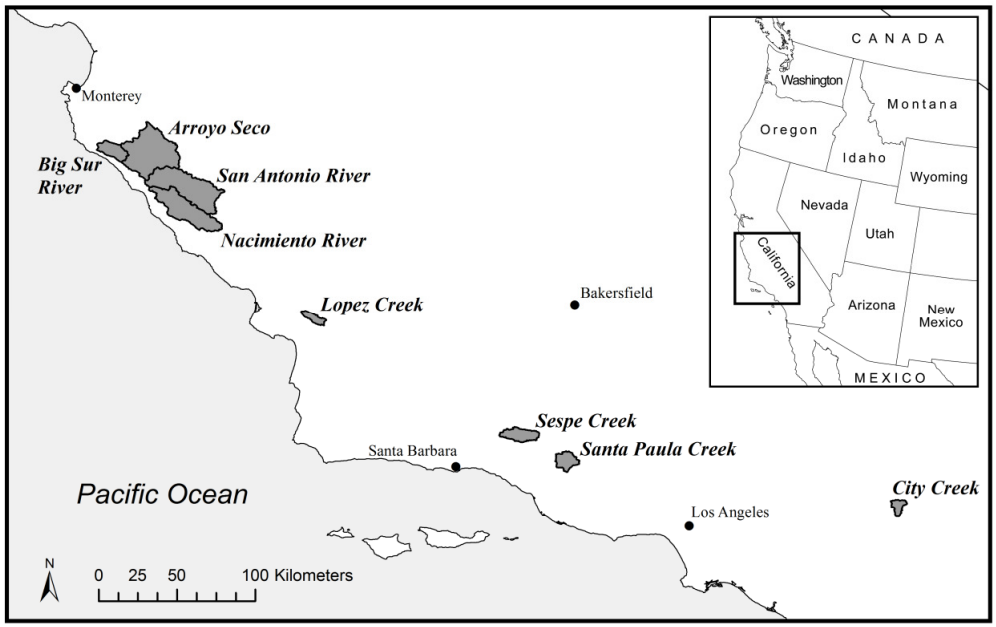

Figure 15: Location of study watersheds in California.

Wildfire characteristics for each watershed are provided in Table 9. The percentage of area burned varied from 20% to 100% of the watershed area. The average length of the pre-fire period was 16.5 years, ranging from 11 to 19 years. A post-fire length of seven years was used for all watersheds except Nacimiento, which had only three years of post-fire data available.

Table 8: Summary of watershed characteristics

Watershed Name	USGS ID	Area (km^2)	Mean annual precipitation (mm)	Mean annual PET (mm)	Mean annual streamflow (mm)	Dominant geology type
Arroyo Seco	11152000	625.1	809	664	243	Sedimentary
Big Sur River	11143000	120.6	1163	640	753	Granitic
City Creek	11055801	50.5	781	729	226	Quarternary
Lopez Creek	11141280	54.0	717	741	170	Sedimentary
Nacimiento River	11148900	403.5	692	745	409	Sedimentary
San Antonio River	11149900	556.4	633	737	174	Sedimentary
Santa Paula Creek	11113500	103.3	678	709	220	Sedimentary
Sespe Creek	11111500	128.5	850	552	120	Sedimentary

Watershed Name	Stream density (km/Km^2)	Mean slope (%)	Mean soil depth (mm)	Mean clay percentage	Mean silt percentage	Shrubland percentage
Arroyo Seco	1.03	34.7	644	20.2	34.8	42.2
Big Sur River	0.98	43.6	633	14.1	31.5	33.1
City Creek	1.21	34.4	650	13.2	30.6	77.5
Lopez Creek	0.69	37.1	658	32.6	38.8	27.8
Nacimiento River	0.99	21.3	720	22.9	36.9	40.8
San Antonio River	1.13	19.5	862	24.4	37.8	39.1
Santa Paula Creek	1.18	34.4	621	23.6	44.2	55.6
Sespe Creek	1.25	26.5	573	22.1	41.3	45.9

Table 9: Fire characteristics, analysis periods and calibration variables

Catchment	Fire Year	Fire Size (%)	Pre-fire Period	Post-fire Period	Pre-fire events	Post-fire events	Median *b* value	ΔQ_{Crit}
Arroyo Seco	1977	63	1967-1977	1978-1984	42	45	2.058	0.1
Big Sur	1977	92	1967-1977	1978-1984	41	38	1.985	0.25
City	2003	94	1986-2003	2004-2010	27	11	1.872	0.4
Lopez	1985	100	1968-1985	1986-1992	26	4	1.716	0.4
Nacimiento	1996	20	1980-1996	1997-1999	95	17	1.954	0.1
San Antonio	1985	31	1967-1985	1986-1992	73	17	1.658	0.12
Santa Paula	1985	71	1967-1985	1986-1992	41	10	1.782	0.2
Sespe	1985	40	1967-1985	1986-1992	30	8	1.884	0.2

4.4. Methodology

4.4.1. Derivation of baseflow recession rates

Baseflow recession curves were defined as a consecutive decline in the streamflow hydrograph for five or more days following the exclusion of the first two days after a hydrograph stormflow peak. A daily precipitation threshold of 5mm during the recession period was also included to account for precipitation events that may have decreased baseflow recession rates but not increased baseflow volumes.

While baseflow recession curves may be analyzed directly from the recession limb of a streamflow hydrograph using an exponential or non-linear model (Chapman, 1999; Wittenberg, 1999), Brutsaert and Nieber (1977) proposed comparing the rate of baseflow change dQ/dt to baseflow magnitude Q on a $\log(-dQ/dt) - \log(Q)$ plot. This relation is represented as

$$-\frac{dQ}{dt} = f(Q). \tag{18}$$

The time variable is eliminated using this approach, allowing baseflow recession rates for a given baseflow magnitude to be comparable between baseflow recession curves. This relation is referred to as the recession slope curve (Rupp and Selker, 2006a) and frequently follows a power-law function

$$-\frac{dQ}{dt} = aQ^b \tag{19}$$

where Q is baseflow discharge in mm, t is time (daily), a is the value of $-dQ/dt$ when $Q = 1$ and b is the slope of the $\log(-dQ/dt) - \log(Q)$ relation (Clark et al., 2009). dQ/dt was computed as the difference between two consecutive points on a baseflow recession curve,

$$\frac{dQ}{dt} = \frac{Q_i - Q_{i-1}}{\Delta t}, \tag{20a}$$

and Q was computed as the mean of two consecutive recession points,

$$Q = \frac{Q_i + Q_{i-1}}{2}. \tag{20b}$$

Low precision in the gauging of low flows may hinder investigations of the recession slope curve due to scatter and discretization associated with low magnitude recession flows on a $\log(-dQ/dt) - \log(Q)$ plot. These errors were accounted for by increasing the time interval Δt for flows below the precision of the gauge until the change in baseflow ΔQ over the time-period exceeded a critical threshold ΔQ_{crit} (Rupp and Selker, 2006b). The critical threshold was determined visually for each watershed (Table 9).

Previous studies have demonstrated that values of b in the power-law relation of Equation 19 are less variable than values of a (Shaw et al., 2013). In this study, the exponent b was fixed at a common value for each watershed, leaving a single free parameter a for representing baseflow recession rates. The fixed value of b was

derived by fitting a linear regression model with log-transformed data (Xiao et al., 2011) to each individual recession slope curve in a watershed and selecting the median *b* value from among all the curves (Table 9). *a* was then recomputed for all values along the recession slope curve using Equation 19 with the fixed b. The median value of *a* from each individual recession slope curve was used to represent the baseflow recession rate for that recession slope curve.

4.4.2. Mixed model

A model is often used to isolate the effect of wildfire on baseflow recession rates from other potential sources of variability. Linear regression is the most commonly used statistical model for this purpose. However, baseflow recession curve data contains a hierarchical structure that violates the assumption of independence that is required for linear regression models (Watson et al., 2001). At the watershed scale, baseflow recession rates within a given year are likely to be more similar than between years. This multiple-level organization within the data produces the hierarchical structure. Baseflow recession rates represent the lower level of the hierarchy (i.e. level 1) and are considered to be nested within years, which represent the higher level of the hierarchy (i.e. level 2) (Figure 16). At the regional scale, the hierarchical structure becomes more complex, with baseflow recession rates nested within years which are then nested within watersheds (Figure 16). This type of hierarchical structure is referred to as having three levels. Baseflow recession rates at the regional scale may alternatively be considered to be nested by precipitation event

(Figure 16). Watersheds with baseflow recession rates produced from the same precipitation event will likely be more similar than baseflow recession rates produced from different precipitation events due to similarities in antecedent storage across a region. Data with two hierarchical structures is commonly referred to as having crossed-random effects (Baayen et al., 2008).

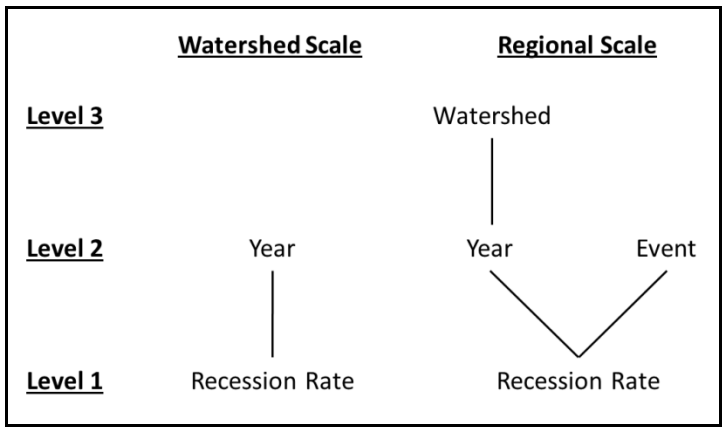

Figure 16: Hierarchical structure for watershed-scale and regional-scale mixed models.

Mixed modeling is a technique used to examine data containing a hierarchical structure. Mixed models may be referred to as multilevel models, hierarchical models, generalized linear mixed models (GLMM), mixed-effects models and meta-analysis (Hox, 2010). Mixed models account for hierarchies within data by partitioning model error to each level of the hierarchy using variables containing random effects. Random effects represent the stochastic portion of the model, as opposed to the fixed effects which represent the deterministic portion of the model (Hox, 2010). A mixed model for representing the watershed-scale hierarchy in Figure 16 may be described as

$$y_{ij} = \beta_0 + u_j + e_{ij} \quad (21)$$

where y_{ij} is the *i*th observation of baseflow recession rates (*a*) for the *j*th year, β_0 is the intercept of the model, u_j is the level-2 model error for the the *j*th year and e_{ij} is the level-1 model error for the *i*th observation from the *j*th year. Including level-1 predictor variables, the mixed model may be described as

$$y_{ij} = \beta_0 + \sum_{n=1}^{N} \beta_n x_{nij} + u_j + e_{ij} \quad (22)$$

where *N* is the total number of predictor variables, β_n is the slope of the relation between the *n*th predictor variable and baseflow recession rates, and x_{nij} is the *i*th observation of the *n*th predictor variable for the *j*th year.

Model errors in mixed models are generally assumed to be independent and normally distributed with a mean of 0 and a variance of σ^2. However, autocorrelation of level-1 model errors may occur with longitudinal data such as baseflow recession rates if memory from one baseflow recession event affects subsequent events. In some cases, this autocorrelation may be explicitly modeled through the error covariance matrix (Hox, 2010). However, when the available data at the lowest hierarchical level is small, quantifying the autocorrelation can be challenging. Fortunately, the effect of autocorrelation on mixed modeling results, and particularly the fixed effects, has been shown to be negligible when level-1 sample sizes are small

(Hox, 2010; Raudenbush and Bryk, 2002). The median number of baseflow recession events within a given year for this study was 3, ranging from 1 to 11. Since the primary objective was to understand how a fixed-effect variable, fire, affects baseflow recession rates, level-1 autocorrelation was not explicitly accounted for in this study.

A mixed model for representing the regional-scale hierarchy in Figure 16 may be represented by

$$y_{i(jk\cdot l)} = \beta_0 + w_l + v_k + u_{jk} + e_{i(jk\cdot l)} \tag{23}$$

where $y_{i(jk\cdot l)}$ is the *i*th observation of baseflow recession rate from the cross-classified *j*th year and *k*th watershed with the *l*th precipitation event, w_l is the level-2 model error for the *l*th precipitation event, v_k is the level-3 model error for the *k*th watershed, u_{jk} is the level-2 model error for *j*th year in the *k*th watershed, and $e_{i(jk\cdot l)}$ is the level-1 model error for the *i*th observation of baseflow recession rate from the cross-classified *j*th year and *k*th watershed with the *l*th precipitation event (Hox, 2010). The model including level-1 predictor variables is

$$y_{i(jk\cdot l)} = \beta_0 + \sum_{n=1}^{N} \beta_n x_{ni(jk\cdot l)} + w_l + v_{0k} + u_{0j} + e_{i(jk\cdot l)} \tag{24}$$

where $x_{ni(jk\cdot l)}$ is the *i*th observation for the *n*th predictor variable from the cross-classified *j*th year and *k*th watershed with the *l*th precipitation event.

A Bayesian estimation procedure using Markov Chain Monte Carlo (MCMC) techniques was used to calibrate the mixed model (Stegmueller, 2013). A Gibbs sampling algorithm with an improper, non-informative prior was applied for each MCMC walk (Hadfield, 2010). A total of 1,000,000 iterations with a thinning of 100 were conducted following a burn-in period of 20,000. All modeling was implemented in the R programming language (www.r-project.org) using the MCMCglmm package (Hadfield, 2010). Model fit was evaluated using the Deviance Information Criterion (DIC) (Hadfield, 2010). DIC is obtained from

$$DIC = \overline{D} + p_D. \tag{25}$$

$\overline{D}$ is the average deviance D over all MCMC iterations, with deviance is defined as

$$D = -2\ln(p(y|\theta)). \tag{26}$$

$p(y|\theta)$ is the likelihood function and θ is a parameter of the model. p_D is a measure of the effective number of parameters (Spiegelhalter et al., 2002). Models with smaller values of DIC indicate better model fit.

4.4.3. Model development

To examine the effect of wildfire on baseflow recession rates, watershed-specific (Equation 22) and region-specific (Equation 24) models were developed to predict a (logged base e) from three watershed variables; antecedent storage (logged base e), potential ET and fire. These variables were selected a-priori based on the

hydrological processes that were expected to be important controls on baseflow recession rates, with antecedent storage and potential ET being key controls on inter-seasonal baseflow recession rates and fire being the primary variable of interest.

The seasonality of rainfall in California produces two different hydrologic regimes; a water-limited summer dry season and an energy-limited winter wet season. In Chapter 3 it was shown that baseflow recession rates in central California watersheds decrease as watershed storages are filled during the transition from the dry season to the wet season. To account for inter-seasonal differences in antecedent storage for this study, an estimate of antecedent storage for each baseflow recession event was developed using precipitation cumulated from the beginning of the wateryear (October 1) to the start of each baseflow recession curve. This proxy for antecedent storage is similar to that used in Chapter 3, but with precipitation substituted for streamflow since streamflow is a component of the dependent variable in the mixed model. While cumulative antecedent precipitation cannot account for decreases in watershed storage between precipitation events, it was assumed that cumulative antecedent precipitation would provide a first-order approximation of antecedent storage for each recession event.

Potential ET was derived from daily temperature data using the Blaney-Criddle transformation;

$$PET = p(0.457 * T + 8.13) \quad (27)$$

where *PET* is the estimated potential ET (mm/day), *T* is the mean daily temperature (°C) and *p* is the mean daily percentage of total annual daytime hours at 35 degrees latitude (Blaney and Criddle, 1962).

The effect of wildfire on baseflow recession rates was incorporated into the model via a fire variable representing watershed conditions before and after wildfire. Watershed conditions during the pre-fire period were assumed to be stable and uniform. For the first post-fire year, the change in watershed conditions was assumed to be equivalent to the percentage of watershed area burnt. For subsequent post-fire years, the level of change in watershed conditions was based on the reverse scaling (i.e. 1 minus value) of the normalized post-fire vegetation recovery curve introduced in Chapter 2 and developed from two remote sensing studies of chaparral recovery in central California (Hope et al., 2007; McMichael et al., 2004). The normalized post-fire vegetation recovery curve was computed as {0.00, 0.37, 0.50, 0.60, 0.68, 0.75, 0.81} for the first seven years following fire, with the interval between 0 and 1 representing post-fire vegetation decrease during the first post-fire year and pre-fire conditions, respectively. This fire variable was found to be the best predictor of post-fire annual streamflow in California watersheds from several fire variables tested in Chapter 2.

To examine how antecedent storage and potential ET modify baseflow recession rate response to wildfire, two interaction variables were separately incorporated into the model. An interaction variable between fire and antecedent storage was as generated from the product of the fire variable with the cumulative

antecedent precipitation variable. An interaction variable between fire and potential ET was generated from the product of the fire variable with the potential ET variable.

For mixed models, predictor variables are often rescaled to contain a zero point in order to aid in the interpretation of model results (Enders and Tofighi, 2007). To establish a zero point, predictor variables are centered by subtracting the mean value of the predictor variable. Two types of centering may be implemented based on the strategy for selecting the mean value of the predictor variable. Grand mean centering centers a variable about its grand mean, while group mean centering centers a variable about the mean of the group to which each value is associated (Enders and Tofighi, 2007). The two forms of centering may produce different model interpretations (Aguinis et al., 2013). Following the recommendation of Enders and Tofighi (2007), for models directly investigating the effect of wildfire on baseflow recession rates (i.e. primary objective), cumulative antecedent precipitation and potential ET were grand-mean centered for the watershed-scale models and group-mean centered by watershed for the regional-scale models. For all models investigating how interaction variables may modify the effect of wildfire on baseflow recession rates, cumulative antecedent precipitation and potential ET were group-mean centered by wateryear.

4.5. Results and discussion

The relation between baseflow recession rates (a) and cumulative antecedent precipitation for each of the eight watersheds is displayed in Figure 17. Baseflow

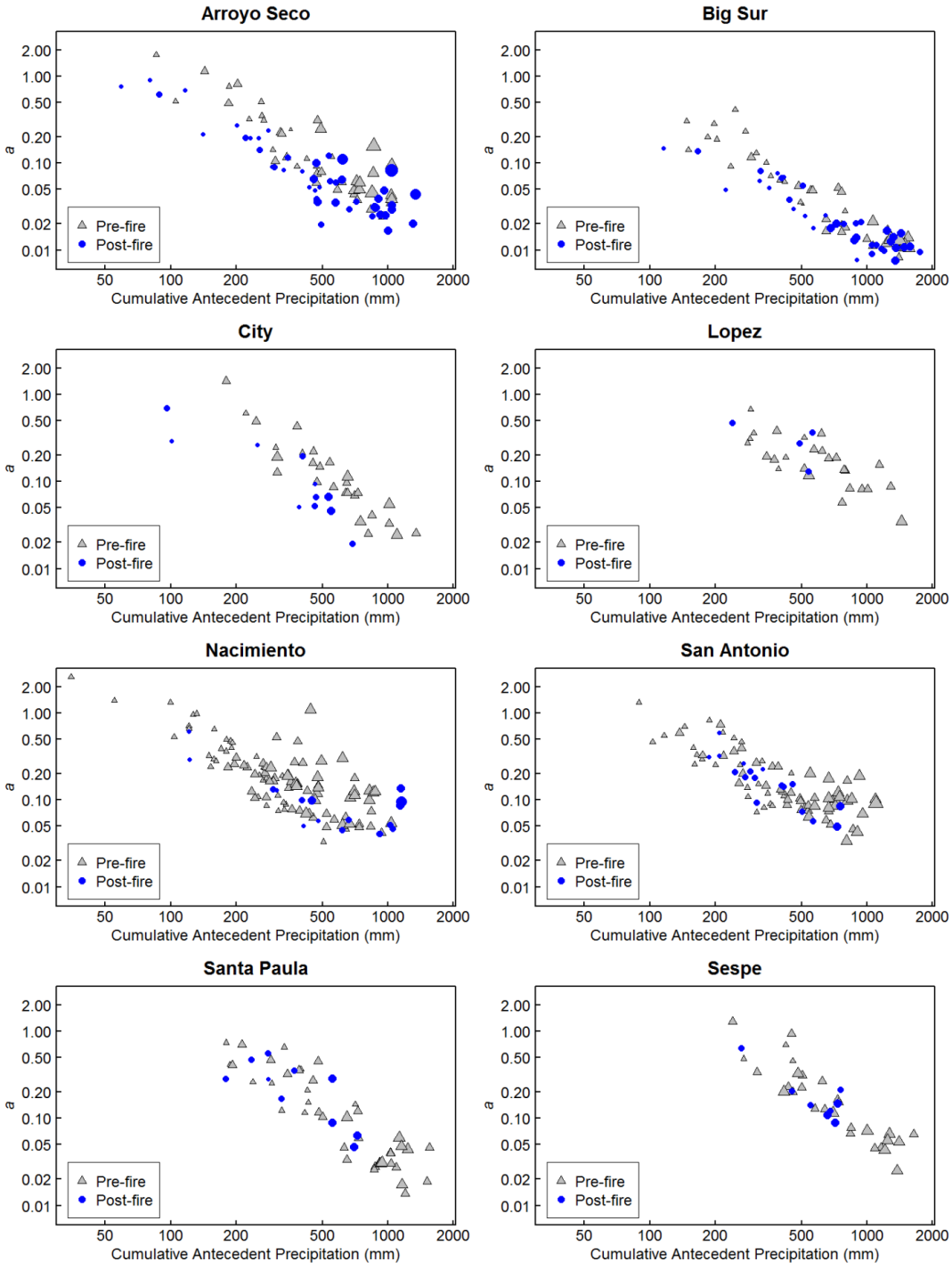

Figure 17: Plots of *a* from Equation 19 against cumulative antecedent precipitation, separated by pre- and post-fire baseflow. Larger symbols correspond to higher potential ET (Range 1.7 to 6.1 mm/day).

recession rates were separated by pre- and post-fire with symbol size corresponding to potential ET levels during the recession event. Baseflow recession rates decreased with higher cumulative antecedent precipitation and the relation between the two variables generally followed a power-law function. Potential ET was also slightly correlated with cumulative antecedent precipitation (Pearson's $r = 0.61$). For a given level of cumulative antecedent precipitation, higher potential ET generally corresponded to a higher value of a, although this effect was not ubiquitous. Post-fire baseflow recession rates decreased relative to pre-fire baseflow recession rates in three watersheds; Arroyo Seco, Big Sur and City. Post-fire baseflow recession rates in the five other watersheds did not exceed the variability of the pre-fire baseflow recession rates.

The values representing the mode and 95% credible (i.e. confidence) intervals for each of the four fixed parameters in the watershed and regional-scale models were grouped by parameter and are presented in Figure 18. Two of the parameters, the intercept and cumulative antecedent precipitation, were highly significant in each of the watersheds and at the regional scale. This reinforces the visual evidence in Figure 17 that baseflow recession rates decrease with higher levels of antecedent storage. For every doubling of cumulative antecedent precipitation, the value of a decreased by 64.6% (62.4% to 67.5%) at the regional scale. The similarity of coefficient values amongst the watersheds suggests that similar controls on inter-seasonal baseflow recession rates operate throughout the study region. These findings mirror those of Chapter 3.

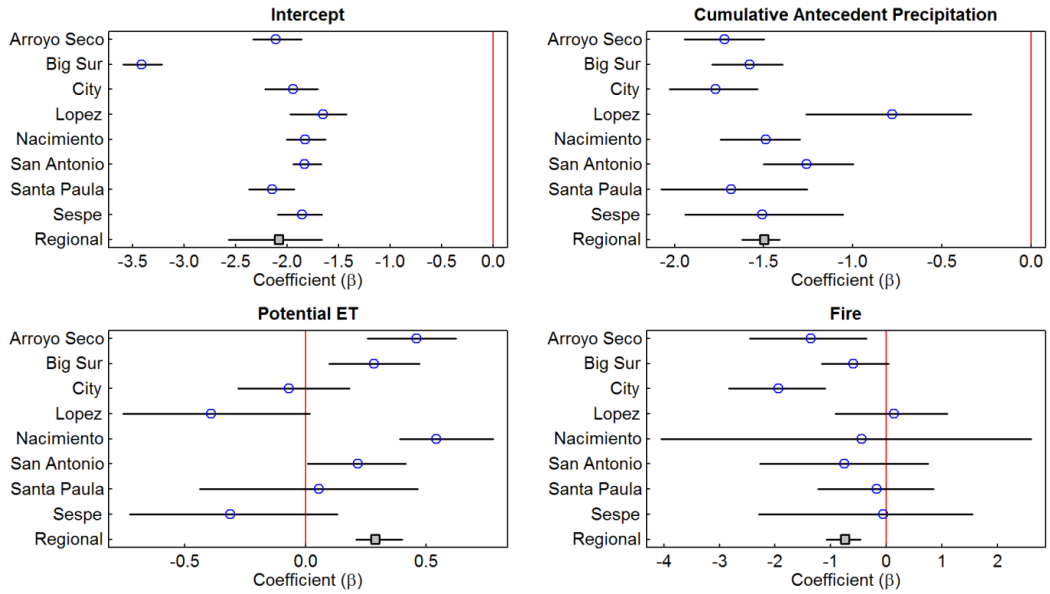

Figure 18: Coefficient (β) values and 95% credible intervals for watershed-scale and regional-scale mixed models. (Regional = Crossed random effects model).

The effect of potential ET on baseflow recession rates was more variable than cumulative antecedent precipitation, with four watersheds showing significant increases in baseflow recession rates with higher levels of potential ET (Figure 18). These four watersheds were clustered in the Santa Lucia Mountains in the northern portion of the study region, suggesting that phreatophytes in this area may have greater contact with groundwater than in the southern watersheds. The lack of significant change observed in the four southern watersheds is supported by a study from Tschinkel (1963) who found the effect of ET on baseflow recession rates to be negligible in a small southern California watershed located to the west of City (Zecharias and Brutsaert, 1988). As the four northern watersheds corresponded to the four watersheds with the most available data (Table 9), the regional effect of potential

ET on baseflow recession rates was found to be statistically significant. The regional model predicted that for every millimeter increase in daily potential ET, the value of *a* would increase by 33.5% (23.2% to 49.1%).

At the watershed scale, baseflow recession rates showed a significant decrease following wildfire in two watersheds, Arroyo Seco and City (Figure 18). Five additional watersheds showed a non-significant decrease in baseflow recession rates. Combined, these results produced a significant regional decrease in post-fire baseflow recession rate, with the regional-scale model predicting that baseflow recession rates would decrease 52.5% (37.6% to 66.0%) during the first post-fire year assuming 100% burnt. This decrease in baseflow recession rate implies that an increase in net flux to groundwater during the recession period occurs following fire; either through decreased groundwater ET, decreased soil ET, and/or decreased interception. The primary process operating in City may have been increased groundwater recharge resulting from decreased interception since baseflow recession rates showed a large decrease following fire but no response to changes in potential ET. Baseflow recession rates in Arroyo Seco, on the other hand, were very responsive to changes in potential ET, suggesting that decreased groundwater ET and/or decreased soil ET following fire may have been an important control on baseflow recession rates in that watershed.

An interaction variable testing the effect of inter-seasonal differences in cumulative antecedent precipitation on post-fire baseflow recession rate change is shown in Figure 19. For two watersheds, Arroyo Seco and Big Sur, greater post-fire

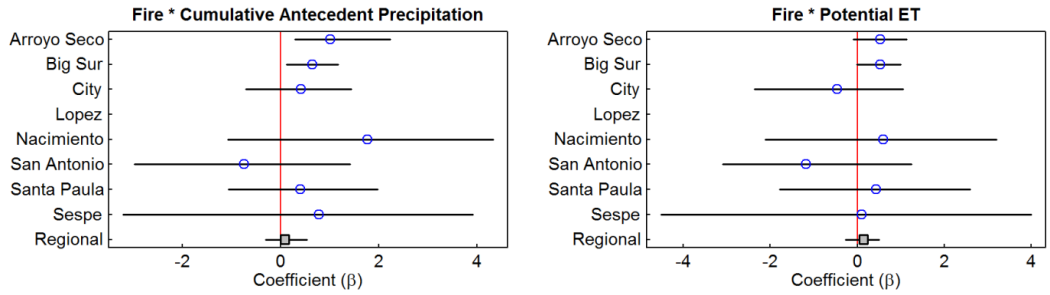

Figure 19: Coefficient (β) values and 95% credible intervals for interaction variables.

baseflow recession rate change was observed with lower cumulative antecedent precipitation than with higher cumulative antecedent precipitation. This effect may be the result of inter-seasonal differences in the dominant controls on baseflow recession rates. In Chapter 3, the primary control on baseflow recession rates in California watersheds was found to shift from small, quickly-recharged groundwater stores early in the wet season to larger, seasonal groundwater stores later in the wet season. For a given ET flux from groundwater, the effect on storage depletion will be proportionally larger for a small store than a large store. Therefore, the effect of wildfire on baseflow recession rates could be expected to be greatest early in the wet season for California watersheds containing phreatophyte vegetation. None of the watershed-scale models besides Arroyo Seco and Big Sur, or the regional-scale model, showed significant changes in post-fire baseflow recession rate response with cumulative antecedent precipitation (no value was obtained for Lopez). The large credible intervals associated with many of the watershed-scale models suggests that the statistical power for evaluating these models may have been weak, possibly due to

an insufficient amount of available post-fire data. As a result, the overall effect of antecedent storage on post-fire baseflow recession rate change remains inconclusive.

The effect of potential ET on post-fire baseflow recession rate change was small and insignificant at both watershed and regional scales (Figure 19). Collectively, many of the coefficient values point to a decrease in baseflow recession rate response to wildfire with increasing potential ET. However, this effect is opposite of what would be expected based on the physical processes operating in a watershed. These results once again suggest that the available data in this study may not support the complexity of the mixed model when an interaction term is included.

4.6. Conclusions

The purpose of this paper was to examine the impact of fire on baseflow recession rates. The first-order control on baseflow recession rates was found to be inter-seasonal differences in antecedent storage, with baseflow recession rates decreasing with increasing cumulative antecedent precipitation. Baseflow recession rates also increased with higher levels of potential ET, although this effect was highly variable at the watershed scale. At a regional scale, wildfire decreased baseflow recession rates 52.5% (37.6% to 66.0%) during the first post-fire year assuming 100% burnt. This decrease implies that processes associated with post-fire reductions in above-ground vegetation (e.g. decreased interception, decreased soil ET, decreased groundwater ET) were the dominant hydrologic controls on baseflow recession rates. The effect of wildfire on baseflow recession rates was not sensitive to inter-seasonal

differences in post-fire antecedent storage or potential ET. However, more data will be needed to conclusively assess this latter result due to weak statistical power for evaluating the interaction variables.

The results of this study indicate that baseflow recession rates decrease following wildfire at a regional scale; at a watershed scale, the level of decrease was more variable. To better predict watershed to watershed differences in baseflow recession rate response to fire in the future, it will be necessary to 1) identify areas within a watershed that contain phreatophytes vegetation and 2) quantify burn severity in these areas. In the current study, area burnt was evaluated relative to the entire watershed and all burnt areas were assumed to have equal burn severity. By identifying locations within the watershed containing phreatophyte vegetation and using satellite data such as the Moderate Resolution Imaging Spectroradiometer (MODIS) to estimate burn severity, uncertainty in the prediction of baseflow recession rates response to fire may be reduced.

4.7. References

Aguinis, H., Gottfredson, R.K., Culpepper, S.A., 2013. Best-Practice Recommendations for Estimating Cross-Level Interaction Effects Using Multilevel Modeling. Journal of Management 39, 1490–1528. doi:10.1177/0149206313478188

Aksoy, H., Wittenberg, H., 2011. Nonlinear baseflow recession analysis in watersheds with intermittent streamflow. Hydrological Sciences Journal 56, 226–237. doi:10.1080/02626667.2011.553614

Baayen, R.H., Davidson, D.J., Bates, D.M., 2008. Mixed-effects modeling with crossed random effects for subjects and items. Journal of memory and language 59, 390–412.

Bickel, R., 2007. Multilevel analysis for applied research: It's just regression! The Guilford Press.

Blaney, H.F., Criddle, W.D., 1950. Determining water requirements in irrigated areas from climatological and irrigation data (No. SCS-TP 96). U.S. Dept. Agriculture Soil Conservation Service.

Blaney, H.F., Criddle, W.D., 1962. Determining consumptive use and irrigation water requirements, Technical Bulletin. US Department of Agriculture.

Brutsaert, W., Nieber, J.L., 1977. Regionalized drought flow hydrographs from a mature glaciated plateau. Water Resources Research 13, 637–643.

Callaway, R.M., Davis, F.W., 1993. Vegetation Dynamics, Fire, and the Physical Environment in Coastal Central California. Ecology 74, 1567–1578. doi:10.2307/1940084

Cannon, S.H., Gartner, J.E., Wilson, R.C., Bowers, J.C., Laber, J.L., 2008. Storm rainfall conditions for floods and debris flows from recently burned areas in southwestern Colorado and southern California. Geomorphology 96, 250–269.

Clark, M.P., Rupp, D.E., Woods, R.A., Tromp-van Meerveld, H.J., Peters, N.E., Freer, J.E., 2009. Consistency between hydrological models and field observations: linking processes at the hillslope scale to hydrological responses at the watershed scale. Hydrological Processes 23, 311–319.

Colman, E.A., 1951. Fire and water in southern California's mountains (California Forest and Range Experiment Station, US Department of Agriculture-Forest Service, Miscellaneous Paper #3).

Crouse, R.P., 1961. First-year effects of land treatment on dry-season streamflow after a fire in southern California (Research Note #191). USDA Forest Service, Pacific Southwest Forest and Range Experiment Station, Berkeley, California.

DeBano, L.F., 2000. The role of fire and soil heating on water repellency in wildland environments: a review. Journal of Hydrology 231-232, 195–206. doi:10.1016/S0022-1694(00)00194-3

Doerr, S.H., Shakesby, R.A., Walsh, R.P.D., 2000. Soil water repellency: its causes, characteristics and hydro-geomorphological significance. Earth-Science Reviews 51, 33–65. doi:10.1016/S0012-8252(00)00011-8

Enders, C.K., Tofighi, D., 2007. Centering predictor variables in cross-sectional multilevel models: a new look at an old issue. Psychological methods 12, 121.

Falcone, J.A., 2011. GAGES-II: geospatial attributes of gages for evaluating streamflow. Digital spatial data set.

Hadfield, J.D., 2010. MCMC methods for multi-response generalized linear mixed models: the MCMCglmm R package. Journal of Statistical Software 33, 1–22.

Hope, A., Decker, J., Jankowski, P., 2008. Utility of Gridded Rainfall for IHACRES Daily River Flow Predictions in Southern California Watersheds. Journal of the American Water Resources Association (JAWRA) 44, 428–435.

Hope, A., Tague, C., Clark, R., 2007. Characterizing post-fire vegetation recovery of California chaparral using TM/ETM+ time-series data. Int. J. of Remote Sensing 28, 1339–1354. doi:10.1080/01431160600908924

Hox, J., 2010. Multilevel analysis: Techniques and applications. Routledge Academic.

Imeson, A.C., Verstraten, J.M., van Mulligen, E.J., Sevink, J., 1992. The effects of fire and water repellency on infiltration and runoff under Mediterranean type forest. CATENA 19, 345–361. doi:10.1016/0341-8162(92)90008-Y

Jung, H.Y., Hogue, T.S., Rademacher, L.K., Meixner, T., 2009. Impact of wildfire on source water contributions in Devil Creek, CA: evidence from end-member mixing analysis. Hydrol. Process. 23, 183–200. doi:10.1002/hyp.7132

Keller, E.A., Valentine, D.W., Gibbs, D.R., 1997. Hydrological response of small watersheds following the Southern California Painted Cave Fire of June 1990. Hydrological Processes 11, 401–414.

Kinoshita, A.M., Hogue, T.S., 2011. Spatial and temporal controls on post-fire hydrologic recovery in Southern California watersheds. Catena 87, 240–252.

Luce, C., Morgan, P., Dwire, K., Isaak, D., Holden, Z., Rieman, B., 2012. Climate change, forests, fire, water, and fish: Building resilient landscapes, streams, and managers. US Department of Agriculture, Forest Service, Rocky Mountain Research Station.

McMichael, C.E., Hope, A.S., 2007. Predicting streamflow response to fire-induced landcover change: Implications of parameter uncertainty in the MIKE SHE model. Journal of Environmental Management 84, 245–256. doi:10.1016/j.jenvman.2006.06.003

McMichael, C.E., Hope, A.S., Roberts, D.A., Anaya, M.R., 2004. Post-fire recovery of leaf area index in California chaparral: a remote sensing-chronosequence approach. International Journal of Remote Sensing 25, 4743–4760. doi:10.1080/01431160410001726067

Meixner, T., Wohlgemuth, P.M., 2003. Climate variability, fire, vegetation recovery, and watershed hydrology, in: Proceedings of the First Interagency Conference on Research in the Watersheds. Benson, Arizona, pp. 651–656.

Raudenbush, S.W., Bryk, A.S., 2002. Hierarchical linear models: Applications and data analysis methods, 2nd ed. Sage, Thousand Oaks, California.

Rundel, P.W., 2004. Mediterranean-climate ecosystems: defining their extent and community dominance, in: Arianoutsou, Papanastasis (Eds.), Proceedings 10th

MEDECOS Conference, Proceedings 10th MEDECOS Conference. Presented at the 10th MEDECOS Conference, Rhodes, Greece, pp. 1–12.
Rupp, D.E., Selker, J.S., 2006a. On the use of the Boussinesq equation for interpreting recession hydrographs from sloping aquifers. Water Resour. Res. 42, W12421.
Rupp, D.E., Selker, J.S., 2006b. Information, artifacts, and noise in dQ/dt - Q recession analysis. Advances in Water Resources 29, 154–160. doi:10.1016/j.advwatres.2005.03.019
Shakesby, R.A., Doerr, S.H., 2006. Wildfire as a hydrological and geomorphological agent. Earth Science Reviews 74, 269–307.
Shaw, S.B., McHardy, T.M., Riha, S.J., 2013. Evaluating the influence of watershed moisture storage on variations in baseflow recession rates during prolonged rain-free periods in medium-sized catchments in New York and Illinois, USA. Water Resour. Res. 49, 6022–6028. doi:10.1002/wrcr.20507
Silberstein, R.P., Dawes, W.R., Bastow, T.P., Byrne, J., Smart, N.F., 2013. Evaluation of changes in post-fire recharge under native woodland using hydrological measurements, modelling and remote sensing. Journal of Hydrology 489, 1–15. doi:10.1016/j.jhydrol.2013.01.037
Spiegelhalter, D.J., Best, N.G., Carlin, B.P., Linde, A. van der, 2002. Bayesian Measures of Model Complexity and Fit. Journal of the Royal Statistical Society. Series B (Statistical Methodology) 64, 583–639. doi:10.2307/3088806
Stegmueller, D., 2013. How Many Countries for Multilevel Modeling? A Comparison of Frequentist and Bayesian Approaches. American Journal of Political Science.
Tague, C., Grant, G.E., 2009. Groundwater dynamics mediate low-flow response to global warming in snow-dominated alpine regions. Water Resour. Res. 45, W07421. doi:200910.1029/2008WR007179
Tallaksen, L.M., 1995. A review of baseflow recession analysis. Journal of Hydrology 165, 349–370. doi:10.1016/0022-1694(94)02540-R
Tschinkel, H.M., 1963. Short-term fluctuation in streamflow as related to evaporation and transpiration. Journal of Geophysical Research 68, 6459–6469.
Watson, F., Vertessy, R., McMahon, T., Rhodes, B., Watson, I., 2001. Improved methods to assess water yield changes from paired-catchment studies: application to the Maroondah catchments. Forest Ecology and Management 143, 189–204.
Wells, W.G., 1987. The effects of fire on the generation of debris flows in southern California. Rev. Eng. Geol 7, 105–114.
Wittenberg, H., Sivapalan, M., 1999. Watershed groundwater balance estimation using streamflow recession analysis and baseflow separation. Journal of Hydrology 219, 20–33.

Xiao, X., White, E.P., Hooten, M.B., Durham, S.L., 2011. On the use of log-transformation vs. nonlinear regression for analyzing biological power laws. Ecology 92, 1887–1894.

Zecharias, Y.B., Brutsaert, W., 1988. Recession characteristics of groundwater outflow and base flow from mountainous watersheds. Water Resources Research 24, 1651–1658.

Chapter 5: Conclusions

This dissertation provided the first regional examination of post-fire streamflow change in California watersheds. In the first paper, Chapter 2, the regional effect of fire on annual streamflow was investigated using a mixed model. At a regional scale, annual streamflow increased significantly following fire. In addition, post-fire annual streamflow response was greatest with higher percentages of watershed area burnt and then decreased as vegetation recovered following fire. The effect of fire on annual streamflow was also sensitive to post-fire annual wetness conditions, with the greatest post-fire increase in annual streamflow occurring during moderately wet years. Methodologically, the mixed modeling approach was found to be a valuable tool for regionalizing post-fire streamflow change from multiple watersheds.

The second and third papers of this dissertation (Chapters 3 and 4) investigated the effect of wildfire on baseflow recession rates. In Chapter 3, the first known study to characterize the relation between inter-seasonal differences in antecedent storage and baseflow recession rates in California was conducted. It was necessary to quantify this relation prior to evaluating the effect of wildfire effect on baseflow recession rates since antecedent storage were observed to be the first-order control on baseflow recession rates. A negative power-law relation was identified between antecedent storage and baseflow recession rates, with baseflow recession rates decreasing by up to an order of magnitude as antecedent storage levels

increased. Simulations using a parsimonious storage-discharge model indicated that this relation may be the product of inter-seasonal differences in the source of recession flows; as the small, quickly-recharged aquifers that dominate baseflow recession response at the beginning of the wet season shift to large, seasonal aquifers as the wet season progresses.

In the third paper (Chapter 4), the effect of wildfire on baseflow recession rates was examined at both watershed and regional scales using the mixed model. This study represented the first comprehensive investigation of the impact of wildfire on baseflow recession rates. As expected, antecedent storage was the most significant control on baseflow recession rates at both scales. The effect of potential ET and wildfire on baseflow recession rates was highly variable at the watershed scale, but both variables were found to be significant controls on baseflow recession rates at the regional scale. For wildfire, post-fire baseflow recession rates decreased by approximately one-half during the first post-fire year assuming 100% area burnt. This decrease implies that the dominant hydrologic control on post-fire baseflow recession rates are related to post-fire reductions in above-ground vegetation in California watersheds (e.g. decreased interception, decreased soil ET, decreased groundwater ET).

5.1. Future research

One of the weaknesses of the regional analyses conducted in this dissertation was the inability to examine the relation between watershed characteristics and post-

fire streamflow change. The number of burnt watersheds available for analysis, twelve and eight for Chapters 2 and 4 respectively, was insufficient to statistically evaluate the impact of watershed characteristics on streamflow response to wildfire. The inclusion of more watersheds would likely improve the analysis. Unfortunately, Bart (2010) has noted that the large number of wildfires in California limits the availability of suitable watersheds with pre- and post-fire periods free of additional wildfires. One potential solution to this limitation may be to include watersheds from other Mediterranean Climate Regions (e.g. South Africa, Australia). This inter-regional approach would increase sample size and could easily be integrated into the mixed modeling framework, with region acting as an additional level of the hierarchy. It may also permit the exploration of inter-regional differences in streamflow response to wildfire.

A further shortcoming of the research in this dissertation was the inability to characterize burn severity for phreatophyte vegetation. Post-fire reductions in phreatophytes are likely to be a better predictor of post-fire baseflow recession rates than percentage of watershed area burnt, as used in this study. Identifying both the location of phreatophytes within a watershed and their burn severity may help to reduce uncertainty in baseflow recession rate change experiments. Sensors such as the Moderate Resolution Imaging Spectroradiometer (MODIS) can provide measures of post-fire burn severity for wildfires during the satellite era. Identifying areas within the watershed with phreatophyte vegetation is less straightforward. Nevertheless, riparian zones may provide a satisfactory approximation of

phreatophyte spatial extent and future research may want to investigate the relation between riparian zone burn severity and baseflow recession rate response.

Finally, the regional analyses in this dissertation demonstrated the applicability of the mixed modeling approach for synthesizing empirical data from multiple streamflow change events. Future research on streamflow may wish to extend this modeling approach to other forms of land-cover change and/or climate change. The mixed model is particularly well suited for exploiting large watershed datasets (e.g. MOPEX).

5.2. References

Bart, R., Hope, A., 2010. Streamflow response to fire in large catchments of a Mediterranean-climate region using paired-catchment experiments. J. Hydrol. 388, 370–378.